

5 Volatile organic compound fluxes over a winter wheat field by PTR-Qi-TOF-MS and eddy covariance

Benjamin Loubet^{1,*}, Pauline Buysse¹, Lais Gonzaga-Gomez¹, Florence Lafouge¹, Raluca Ciuraru¹, Céline Decuq¹, Julien Kammer^{1,a}, Sandy Bsaibes^{1,2}, Christophe Boissard^{2,3}, Brigitte Durand¹, Jean-Christophe Gueudet¹, Olivier Fanucci¹, Olivier Zurfluh¹, Letizia Abis^{1,b}, Nora Zannoni^{2,c}, François Truong², Dominique Baisnée², Roland-Sarda Esteve², Michael Staudt⁴ and Valérie Gros².

1 UMR ECOSYS, INRAE, AgroParisTech, Université Paris-Saclay, 78850, Thiverval-Grignon, France.

2 Laboratoire des Sciences du Climat et de l'Environnement, LSCE, UMR CNRS-CEA-UVSQ, IPSL, 91191 Gif-sur-Yvette, Île-de-France, France.

3 Université de Paris and Univ Paris Est Creteil, CNRS, LISA, F-75013 Paris, France

4 CEFE, CNRS, EPHE, IRD, Univ Montpellier, Montpellier, France

a now at : Aix Marseille Univ, CNRS, LCE, Marseille, France.

b now at Technische Universität Berlin, Umweltchemie und Luftreinhaltung, Straße des 17. Juni 135, Berlin, 10623, Germany.

c now at Max-Planck Institute for Chemistry, Hahn-Meitner-Weg 1, 55128 Mainz, Germany

* Corresponding author: Benjamin.Loubet@inrae.fr

Abstract. Volatile organic compounds (VOCs) contribute to air pollution through the formation of secondary aerosols and ozone, and extend the lifetime of methane in the atmosphere. Tropospheric VOCs originate to 90% from biogenic sources on a global scale, mainly from forests. Crops are also a potentially large yet poorly characterised source of VOCs (30% of the VOC emissions in Europe, mostly oxygenated). In this study, we investigated VOC fluxes over a winter wheat field by eddy covariance using a PTR-Qi-TOF-MS with high sensitivity and mass resolution. The study took place near Paris over a 5 weeks period and included flowering, crop maturity and senescence. We found a total of 123 VOCs with fluxes three times above the detection limit. Methanol was the most emitted compound with an average flux of $63 \mu\text{g m}^{-2} \text{h}^{-1}$, representing about 52% of summed VOC emissions on a molar basis (36% on a mass basis). We also identified ethanol, acetone, acetaldehyde, and dimethyl sulphide among the six most emitted compounds. The third most emitted VOC corresponded to the ion m/z 93.033. It was tentatively identified as furan ($\text{C}_6\text{H}_4\text{O}$), a compound not previously reported to be strongly emitted by crops. The average summed VOC emissions were about $173 \pm 6 \mu\text{g m}^{-2} \text{h}^{-1}$, while the average VOC depositions were about $109 \pm 2 \mu\text{g m}^{-2} \text{h}^{-1}$, hence 63% of the VOC emissions on a mass basis. The net ecosystem flux of VOCs was an emission of $64 \pm 6 \mu\text{g m}^{-2} \text{h}^{-1}$ ($0.5 \pm 0.05 \text{ nmol m}^{-2} \text{ s}^{-1}$). The most depositing VOC were identified as hydroxyacetone, acetic acid and fragments of oxidised VOCs. Overall, our results reveal that wheat fields represent a non-negligible source and sink of VOCs to be considered in regional VOC budgets, and underline the usefulness and limitations of eddy covariance measurements with a PTR-Qi-TOF-MS.

Keywords: VOC, crop, flux, eddy covariance, methanol, DMS, deposition, emission

1 Introduction

40 Volatile organic compounds (VOCs) are key compounds for atmospheric chemistry that contribute to the production of harmful pollutants to human health, among which ozone (O₃) and secondary organic aerosols (SOA) (Lang-Yona et al., 2010; Monks et al., 2015). Ozone, which is also a powerful greenhouse gas (IPCC, 2018), affects vegetation growth with an estimated annual cost of \$11-18 billion on agricultural production worldwide in the last decade (Ashmore, 2005; Avnery et al., 2011). Similarly, particulate matter (PM) including SOA affects directly and indirectly global warming by modifying radiation scattering and the cloud albedo (Makkonen et al., 45 2012). The official legal directives on VOC emissions are not very restrictive. The main regulations in Europe, resulting from the Gothenburg Protocol of 1999, concern the limitation of their emissions from industrial plants and the limitation of their concentrations in consumer products. The emission of fine particles (PM_{2.5}), on the other hand, are more tightly regulated. European countries must meet air pollution targets set out in the European Air Quality Directive (2008/50/EC). Since VOC are precursors of harmful air pollutants, their sources need to be better 50 quantified to identify potential remedies to mitigate PM_{2.5} and ozone threats.

Of the 760 Tg (C) yr⁻¹ VOC emitted globally, it is estimated that around 90% are from biogenic origin (BVOC) (Sindelarova et al., 2014). Forests are the main emitters and isoprene is the most emitted compound worldwide. In Europe, managed ecosystems (crops, managed grasslands and forests) representing about 50 % of the land area, are the largest VOC source in the continent. According to the European BVOC inventory by Karl et al. (2009a), 55 forests account for 55 % of the total emission, agricultural lands for 27 %, and grasslands, wetlands and shrubs for 18 %. These values are however based on few datasets of BVOC fluxes (Keenan et al., 2009), especially for crops. This leads to uncertainties in the estimates of BVOC fluxes from this type of ecosystem. To date, only a few studies investigated VOC fluxes from crops, most of them by chamber techniques (Copeland et al., 2012; Crespo et al., 2013; Das et al., 2003; Eller et al., 2011; Gonzaga Gomez et al., 2019; Graus et al., 2013; Konig et al., 1995; Wiss 60 et al., 2017). Flux measurements made at canopy level on crops are still rare, and were rather focused on orchards and grasslands (Bachy et al., 2020; Bachy et al., 2018; Bachy et al., 2016; Berhongaray et al., 2017; Brillì et al., 2016; Copeland et al., 2012; Fares et al., 2012; Gallagher et al., 2000; Karl et al., 2001; Karl et al., 2005; Miresmailli et al., 2013; Misztal et al., 2014; Portillo-Estrada et al., 2018; Zenone et al., 2016). Bachy et al. (2016) reported fluxes of isoprene, monoterpenes, methanol, acetone, acetaldehyde and acetic acid from a maize field, 65 which revealed lower emission than those parameterised in VOCs emission models like MEGAN or ORHIDEE (Messina et al., 2016). In a follow-up study, Bachy et al. (2020) reported the first measurements of VOC fluxes above a winter wheat field by eddy covariance with a quadrupole Proton Transfer Mass Spectrometer (PTR-MS). More flux measurements have been reported above grasslands than above crops (e.g.) (Bamberger et al., 2010; Custer and Schade, 2007; Muller et al., 2010; Ruuskanen et al., 2011).

70 Reported VOC emission rates from crops are variable over a wide range of values as shown by Gonzaga et al. (2019) and Bachy et al. (2016). Thus, more data are needed to obtain reliable regional emission estimates. Studies measuring ecosystem scale fluxes are particularly useful, since they integrate VOC sources and sinks throughout the canopy. For example, Bachy et al. (2018) showed that methanol can be emitted from bare agricultural soils in comparable quantities as from plants. The emergence of highly sensitive Time of flight PTR-MS (PTR-TOF-MS) 75 (Sulzer et al., 2014) enables the detection of a lot more VOCs than with previous quadrupole PTR-MS, and allows ecosystem scale measurement of their fluxes by eddy covariance. This opens the possibility to get a much more complete spectrum of VOC fluxes from crops than in previous studies. The objective of this study was therefore

to quantify the fluxes of VOC exchanged between a winter wheat field and the atmosphere at the ecosystem scale using the eddy covariance method, over periods of flowering, grain filling and senescence, using a highly sensitive PTR-Qi-TOF-MS. The methodology to compute the fluxes and their uncertainties are presented in detail, and the emission and deposition fluxes are discussed in terms of their magnitude and timing.

2 Methods

2.1 Experimental site and crop management

Flux measurements took place at the Integrated Carbon Observation System (ICOS) FR-Gri site (Grignon, 48°51'N, 1°58'E) located about 30 km west of Paris (France), over a 46 days period between the 3rd of June and the 19th of July 2016. The site is a 19 ha field (**Figure 1**), with a crop rotation of wheat, maize, barley and occasionally rapeseed, and with a winter cover crop before maize. The soil is classified as Luvisol consisting of 25% clay, 70% silt, and 5% sand. More details about the site can be found in Loubet et al. (2011). The site that is part of a dairy farm receives a lot of nitrogen as mineral or organic matter, which leads to large ammonia volatilisation to the atmosphere (Personne et al., 2015). The field was also shown to be a source of NO (Vuolo et al., 2017) and HONO (Laufs et al., 2016). The field is around 450 m downwind from the farm buildings, with about 250 dairy cows and 900 lambs. The farm has a storage tank for manure and storage areas. The farm buildings were shown to be a large source of ammonia that can be detected from the field site (Loubet et al., 2012). Similarly, Kammer et al. (2020) demonstrated that the animal farm is a consistent source of VOC and especially methanol, ethanol and acetaldehyde, but also a specific source of trimethylamine and dimethylsulfide (DMS) that might hence be detected at the field site.

Winter wheat was sown on 20 October 2015 at a density of 2 500 000 plant ha⁻¹, as a mixture of three varieties (Rubisco, Atlass and Premio). The crop was fertilised 4 times with nitrogen solution (25% NO₃, 25% NH₄, 50% urea) at a rate of 84, 39, 39 and 55 kg N ha⁻¹ on 1 March 2016, 9 April 2016, 29 April 2016 and 10 May 2016. Following the emergence of brown rust or septoria, the crop was sprayed with a fungicide the 13 April 2016 (Cherokee; cyproconazole g L⁻¹, propiconazole 62.5 g L⁻¹, chlorothalonil 375 g L⁻¹, at a rate of 1.25 L ha⁻¹), 16 May 2016 (bixafen 75 g L⁻¹ and prothioconazole 150 g L⁻¹ at a rate of 0.7 L ha⁻¹), and 4 June 2016 (250 g L⁻¹ azoxystrobine at a rate of 0.27 L ha⁻¹). The crop was harvested on 28 July 2016 with a quite small yield of 4.3 10³ kg DW ha⁻¹. The crop started flowering on 20 May and was fully flowered on 1 June 2016. On 9 March 2016 and 28 July 2016, aboveground biomass consisted of 13% and 0% green leaves, 4% and 14% yellow leaves, 65% and 45% stems, and 17% and 41% grain ears, respectively. The maximum LAI of green leaves, indicative of the photosynthesis activity, was 7.3 m² m⁻² on 25 May and decreased to 3.4 m² m⁻² on 9 June. Finally, the canopy height varied from 0.9 to 1.1 m during the experiment with quite large variability inside the field (0.15 m standard deviation).

110



Figure 1. Satellite image of the site showing the ICOS FR-GRI field (yellow line), the ICOS flux station (red dot) the VOC eddy covariance sampling site (blue dot), and the VOC profile sampling site (green dot). The dotted red line shows the Farm buildings where animals are mainly stored, on the southeast of the field. © Google Earth.

115

2.2 Volatile organic compounds measurements

2.2.1 VOC eddy covariance sampling system

VOCs were measured in 30 minutes cycles. The eddy covariance flux was recorded over 20 min, while the last 10 minutes were devoted to vertical profiles (5 min) and chamber (3 min) mixing ratio measurements and zero checks (2 min) by sampling through a hydrocarbon filter. In this study, the profiles and chamber measurements are not presented. A 16-way Sulfinert coated valve, located at 5 cm from the drift tube of the PTR-Qi-TOF-MS and heated to 80°C was used to switch between the eddy covariance and other channels. All sampling tubes were made of Teflon PFA (PerFluoroAlkoxy) surrounded by heating tape inserted in an insulator. Tubes were constantly heated to 60°C using a homemade thermostated device and connected to the PTR-MS inlets heated to 80°C. A stainless steel manifold made of Swagelok T-fittings was used to sub-sample the air from the covariance line to the PTRMS and other instruments. The residence time in the covariance line averaged 2.15 seconds, which consisted of ½-inch tubing (external) flushed with a Busch SV-1010 pump (Busch, SW) with an air flow rate of 42 L min⁻¹. This large flow rate has been set to minimize any chemical reaction and ensure a turbulent flow (Reynolds number ~6000) to keep the high frequency of concentrations fluctuations for the eddy covariance method. The end pressure in the line was 240 mbar below ambient pressure. Air from the covariance line was drawn to the 16-way valve at a rate of 0.5 L min⁻¹ via a 1 m long 1/8 inch external diameter PFA tubing heated to 80°C.

The VOC eddy covariance mast comprised: a sonic anemometer (R3-50, Gill, UK) put at the reference height of 2.7 m above ground, and an open path IRGA for CO₂ and H₂O measurement (Li-7500, LICOR, USA) placed at 0.2 m apart on the east and 0.1 m below the anemometer centre (**Figure 2**). The covariance line head that sampled air to the PTR-Qi-TOF-MS was placed 0.1 m on the east and 0.2 m below the anemometer centre. The eddy covariance line head was made of a stainless steel cup (~2.5 cm diameter with a 1 mm mesh Teflon screen). The covariance line was used for VOC fluxes and mixing ratio measurements as well as for CH₄, N₂O, H₂O, NO_x and

135

O₃ mixing ratios. Ozone and NO_x analysers required a teflonised (internal chambers in Teflon) sub-sampling pump (KNF laboport N820, FR) to increase pressure to ambient.

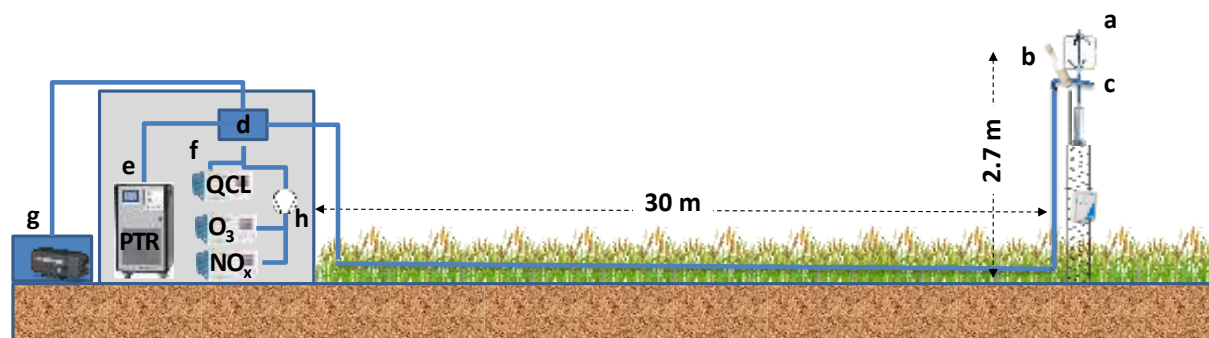


Figure 2. The eddy covariance VOC measurement setup, showing (a) the ultrasonic anemometer, (b) the CO₂ and H₂O open path analyser, (c) the heated sampling line inlet, (d) the heated manifold, (e) the PTR-Qi-TOF-MS, (f) the gas analysers, (g) the high volume vacuum pump, and (h) the teflonised subsampling pump. Diagram not to scale.

2.2.2 PTR-Qi-TOF-MS instrument setup

A PTR-Qi-TOF-MS (Ionicon Analytik GmbH, Innsbruck, Austria) was used for continuous online measurements of VOC mixing ratios at 10 Hz. The analyser was described in detail before (Abis et al., 2018; Sulzer et al., 2014). The drift tube was maintained at 3.5 ± 0.001 mbar and a temperature of $80 \pm 0.16^\circ\text{C}$, while the drift voltage E was set to 995 ± 0.8 V before the 29/06, and to 848 ± 0.3 V after. The corresponding E/N ratios (where E is the electric field strength and N the gas density) were 150.66 ± 0.15 Td and 129.03 ± 0.21 Td (1 Townsend = 10^{-17} V cm⁻²). The E/N ratio at the start of the experiment was rather high and was hence lowered down to 129 Td in the second half of the experiment to minimise cluster formation and fragmentation, although the latter cannot be completely avoided (Pang, 2015; Tani et al., 2003). The number of detection channels was set to 240 000 and the mass spectrum spanned m/z 15 to m/z 530. The extraction rate of ions in the ToF was set to 40 μs (25 kHz), meaning that 2500 extracted spectra were averaged before being recorded at 10 Hz. The mass resolving power corresponded to a resolution (ratio of ion peak width at mid-height to peak value) of around 4500 during the experiment. This means that the instrument had a mass resolving power of ~ 0.007 m/z at $m/z = 30$ and ~ 0.03 m/z at $m/z = 150$.

2.2.3 Acquisition and pre-processing of PTR-Qi-TOF-MS data

A data acquisition software was developed on Labview to synchronize the measurements of the PTR-Qi-TOF-MS with the sonic anemometer and the other fast-response instruments, and to store the data. This software was based on the acquisition of a list of ion peaks integrated online by the TOFDAQ software (TOFWERK, SW) using shared variables that are exchanged between the acquisition computer and the PTR-Qi-TOF-MS computer via a local Ethernet connexion. The desired ion peak list was set up at the start of the experiment based on a list of known compounds tuned to the site. The acquired ion peak integrals counts per seconds (cps) were synchronized at 20 Hz with the ultrasonic anemometer. Every 5 minutes, a mass calibration was performed by the TOFDAQ software using masses m/z 21.0221 (H₃¹⁸O⁺) and m/z 59.049 (acetone C₃H₆OH⁺). When the calibration of these masses shifted from the real masses by more than 0.005 m/z the 5 minutes record was discarded. Additionally, the quality of the peak integration was verified *a posteriori* by integrating several spectra with PTRMS Viewer (Ionicon, V3.3). We found errors lower than 5% for most of the compounds in the most emitted ions as shown by Gonzaga

170 et al., (2019). The synchronized data, stored every five minutes in binary files, were pre-processed with another Labview program to compute the mixing ratios and fluxes.

2.2.4 VOC mixing ratio computation

The pre-processing steps provided averages and standard deviations counts per seconds (cps) for the ion peaks selected R_i . The mixing ratio of the compound $\chi_{i,ptr}$ (in ppb) prior to any calibration, was calculated as:

$$175 \quad \chi_{i,ptr} = 1.657 e^{-11} \times \frac{U_{drift} T_{drift}^2}{k p_{drift}^2} \times \left(\frac{cps_{R_i H^+}^{trans}}{cps_{H_3O^+}^{trans} + cps_{H_2O.H_3O^+}^{trans}} \right) \quad (1)$$

$$cps_{R_i H^+}^{trans} = \frac{TR_{H_3O^+}}{TR_{R_i H^+}} \times cps_{R_i H^+} \quad (2)$$

where U_{drift} is the voltage of the drift tube (V), T_{drift} is the drift tube temperature in Kelvin (K), $cps_{R_i H^+}$ is the cps of the product ion i , $cps_{H_3O^+}$ and $cps_{H_2O.H_3O^+}$ are the cps of the ion source and the first water cluster, k is the proton transfer reaction rate assumed constant for all compounds ($2.5 \cdot 10^{-9} \text{ cm}^3 \text{ s}^{-1}$), *trans* stands for normalised for transmission, $TR_{H_3O^+}$ is the transmission factor for H_3O^+ , $TR_{R_i H^+}$ is the transmission factor for the product ion i , p_{drift} is the pressure in the drift (mbar). The transmission curve from the supplier was used to compute the transmission. $cps_{H_3O^+}^{trans}$ was computed from ion m/z 21.022 ($H_3^{18}O^+$) by multiplying by the isotopic factor of O^{18}/O^{16} in water 487.56, taking the first water cluster as the ion peak m/z 37.028. The constant $1.657 e^{-11}$ was derived from the PTR-MS geometry (supp. mat.).

185 2.2.5 Calibration procedures and uncertainties

The PTR-Qi-ToF-MS calibration factor was measured 5 times during the experiment. To that purpose, we used a standard calibration mixture cylinder containing 102 ppb of benzene, 104 ppb of toluene, and 130 ppb of ethylbenzene and 336 ppb of xylene (122 ppb Ortho, 121 ppb Meta, 123 ppb Para; BTEX, Messer). The gas mixture from this cylinder was diluted with synthetic air (Alphagaz 1, Air Liquide, FR), filtered with a hydrocarbon and humidity filter (Filter Super Clean, final purity=99.9999%, Restek) and a Hydrocarbon Trap (Supelco, Supelpure HC). Two fluorinert coated mass flow controllers (Bronkhorst) were used for dilution to generate mixing ratios from zero to 50 ppb. Fluorinert coating was used to minimise wall effects in the mass flow controller. The background mixing ratio was determined during each calibration using synthetic air passed through a hydrocarbon filter (Supelco ref 22445-12) for 2 minutes, and keeping the last 30 seconds of the record. The background was also determined every 30 minutes by passing ambient air through the same filter to account for the ambient humidity in the zero calibration. The background mixing ratio was determined as the minimum between a 10-days moving minimum of the zero measured every 30 minutes and the zero measured during the calibrations. This procedure was used since the zero air concentration was sometimes much larger than the one measured with filtered ambient air. The zero was then withdrawn from the uncalibrated mixing ratio, providing the zero corrected mixing ratio $\chi_{i,ptr}^* = \chi_{i,ptr} - \chi_{i,ptr}^{zero \text{ air}}$. Eventually, a calibration factor S_i was applied to $\chi_{i,ptr}^*$ to compute the calibrated mixing ratio χ_i , as follows:

$$200 \quad \chi_i = S_i(t) \times \chi_{i,ptr}^* = S_{toluene}(t) \times \frac{S_i(t_0)}{S_{toluene}(t_0)} \times (\chi_{i,ptr} - \chi_{i,ptr}^{zero \text{ air}}) \quad (3)$$

Where $S_{toluene}(t)$ was computed as the slope of the regression (with intercept forced to zero) between $\chi_{i,ptr}^*$ and the prescribed mixing ratio during calibrations was adjusted in time based on the 5 calibrations made during the course of the experiment as well as on E/N and MCP adjustments (see **Table S1**). For the known VOCs, we made a one-off calibration at the start of the experiment the 31 May 2016. Individual calibration factors $S_i(t_0)$ were determined for methanol, acetonitrile, acetaldehyde, ethanol, acroleine, acetone, isoprene, crotonaldehyde, 2butanone, benzene, toluene, o_xylene, chlorobenzene, a_pinen and 1_2_dichlorobenzene (Table S2). In addition, the calibrations factors reported by Koss et al. (2018) were used to compute calibration factors for 145 more compounds (Tables S2). They indeed computed a calibration dataset for a similar, though not exactly identical, instrument as used in this study. They however operated their PTR-TOF-MS instrument with an E/N of 120 Td, which is similar to our setup after the 29/06.

The difference in $S_i(t_0)/S_{toluene}(t_0)$ between Koss et al. (2018) and this study was below 10% for acetaldehyde, acroleine, acetone and benzene, below 50% for methanol, acetonitrile, crotonaldehyde, but only <84% for ethanol, isoprene and monoterpenes. It should be noted that in all cases, $S_i(t_0)/S_{toluene}(t_0) - 1$ has the same sign in both studies. Hence, the calibration factors adopted from that study were good for 4 of 11 compounds and fair for more than half of them. For water vapour, the calibration factor and zero were computed hourly using a linear regression between $\chi_{H2O.H2O.H+,ptr}$ and $\chi_{H2O,Li7500}$.

The relative uncertainty of the calibration factors $\frac{\delta S_i}{S_i}$ was calculated as the sum of relative errors on the linear regressions between prescribed and measured mixing ratios and that of the standard used for calibration. It averaged 12% over the measured VOCs, and was equal to 14.4% for methanol, and 24.3% for ethanol. For the calibration factors taken from Koss et al. (2018), the reported relative uncertainty was used. Overall the relative uncertainty of χ_i was computed following error propagation rules from equation (3):

$$\frac{\delta \chi_i}{\chi_i}(t) = \frac{\delta S_{toluene}}{S_{toluene}}(t) + \frac{\delta S_i}{S_i}(t_0) \quad (4)$$

Where δ denotes an uncertainty. The uncertainty in $\chi_{i,ptr}$ was not considered here as it was assumed to be included in δS_i . The uncertainty of zero air was also neglected compared to the other sources of uncertainty. The relative uncertainty in $S_{toluene}$ is reported in Table S1 and that of S_i in Table S2 (Supp. Mat.).

2.2.6 VOC eddy covariance fluxes computation

The fluxes were computed as the covariance between the vertical component of the wind velocity and the mixing ratio in dry air $\chi_{i,d}$, neglecting the Webb Penman Leuning density correction terms (Leuning, 2007). Indeed, we assumed that the drift temperature was not co-varying with wind velocity, which is a sensible assumption given that the PTR chamber is temperature controlled and given the high thermal mass of the PTR chamber compared to the air mass flowing into the instrument every minute. In these circumstances, the PTR chamber temperature was assumed independent of the air temperature, and the flux was computed as:

$$F_i = \frac{\overline{p_a^d}}{R\overline{T_a}} \overline{w' \chi_{i,d}'} \quad (5)$$

where F_i is the flux ($\text{nmol m}^{-2} \text{s}^{-1}$), $\chi_{i,d}$ is the compound mixing ratio in dry air measured by the PTR (ppb), w is the vertical wind component, $\overline{T_a}$ is the air temperature (K), $\overline{p_a^d}$ the dry air pressure (Pa) and R the ideal gas constant ($8.31 \text{ J mol}^{-1} \text{ K}^{-1}$). Overbars ($\overline{\quad}$) denote averages and primes denote fluctuations following the Reynolds decomposition. Here w' was calculated by applying two rotations following Aubinet et al. (2000). The covariance

between $\chi_{i,d}'$ and w' was calculated after dephasing the two signals with a lag time τ computed as the time at which the correlation function $\overline{w'(t)\chi_{i,d}'(t-\tau)}$ was the largest in absolute value (**Figure S4**). The lag time was set equal for all compounds as the average of the lag time computed for the water cluster, methanol and acetone, which showed very consistent correlation functions between 2.0 and 2.5 s. To compute the covariance, the lag time was

245 constrained between 2.0 and 2.3 s with a fixed value of 2.15 s if the lag exceeded this range as recommended by Langford et al. (2015).

Since the PTR measures a mixing ratio χ_i in wet air, some corrections arise in eq. (5), to account for the dilution of $\chi_{i,d}$ by water vapour. Moreover, since the mixing ratio is computed by normalising with $cps_{H_3O^+}^{trans} + cps_{H_2O.H_3O^+}^{trans}$ (Eqns. 1 and 2), the question also arises as whether this normalisation should be done on raw signal (at 10 Hz) or

250 on averaged signals at 5 min. These two aspects were evaluated by expressing $\chi_{i,d}$ as a function of χ_i and cps_i and differentiating eqns. (1), (2) and (5) (supplementary material section 2). The full expression was derived as a function of water vapour flux and H_3O^+ covariance (Eq. S11). These corrections remained small in our study: lower than 2% each for 75% of the time. Only for a few compounds, the corrections attained 10% for 15% of the time. These included noticeably acetone. We finally derived the Eddy Covariance fluxes, by neglecting the water

255 vapour dilution terms and normalising by H_3O^+ after covariance computation, using the following formula:

$$F_i = S_i \cdot \frac{p_a}{RT_a} \cdot \frac{1.657 e^{-11} U_{drift} T_{drift}^2}{k p_{drift}^2} \cdot \frac{TR_{H_3O^+}}{TR_{R_iH^+} (cps_{H_3O^+}^{trans} + cps_{H_2O.H_3O^+}^{trans})} \cdot \overline{w' cps'_i} \quad (6)$$

Note that the relative uncertainty on the flux is higher than that on the mixing ratio, since it includes both the uncertainty on S_i (see above) and the uncertainty on $\overline{w' cps'_i}$, which includes high frequency losses, and uncertainty of the lag. Overall, the flux was calculated over 85% of the experimental period.

260 2.2.7 High frequency losses

The magnitude of high frequency losses were evaluated as the difference between the cross-spectrum of the first water cluster and air temperature in the high frequency domain, based on the methodology of (Ammann et al., 2006). High frequency losses could not be computed for VOCs due to a too high noise-to-signal ratio, which made the high frequency part of the spectrum non-exploitable for computing the high frequency losses. The loss of signal

265 was starting at a frequency around 0.2 Hz, and the signal was halved at around 2 Hz (**Figure S5**). Since the power-spectral frequency was at around 0.2 Hz at around 14h UTC, the high frequency loss appears just after the spectral peak during the day, but the decrease was gentle until 2Hz and most of the signal energy was contained below 2Hz. The high frequency losses were evaluated by comparing the integrated co-spectra (co-ogives) for water vapour cluster and air temperatures was less than 5%. See Ammann et al. (2006) for details. They were therefore

270 not corrected in the following.

2.2.8 Fluxes limit of detection and VOC flux selection

The limit of detection for fluxes (LOD_f) was determined as the random uncertainty of the eddy covariance method for each compound, which was calculated as the standard deviation of the (w', c') covariance function at +80 s and -80 s as described by Spirig et al. (2005). We chose 80 seconds since our base measurement period was 5

275 minutes, as opposed to Spirig et al. (2005) who used 180 s with a base measurement period of 30 min. This choice should make no difference, since the turbulence decorrelation time at the measurement height is much shorter than 80 s. The VOCs selected for further analysis were those showing an average flux larger than three times the

averaged LOD_f over the entire duration of the experiment. Note that the average LOD_f was calculated as the square root of the sum of the squared individual LOD_f divided by the number of records, to be representative of the error on the mean, as detailed in Langford et al. (2015).

280

2.2.9 Identification of VOC, fragments, clusters and isotopes

Since the PTR-MS only measured a mass to charge ratio m/z , VOCs were tentatively identified by comparing their ion masses with literature values (Yáñez-Serrano et al., 2021). Tentative identifications are summarized in **Table S3**. By analysing correlations between ion peaks, we identified possible fragments and clusters belonging to the same compound. Ions having a Spearman correlation coefficient larger than 0.99 were considered stemming from a same compound. Correlated ions were mostly isotopes or VOCs having m/z peaks too close to each other to be separated by the instrument resolution, but also compounds with a mass difference between 12 and 42 (**Table S4a, b and c**). Therefore, the formaldehyde fluxes (m/z 31.018) reported in the present study should be considered with caution due to uncertainties in its dependence to air humidity.

285

2.3 Meteorological data, CO₂ and energy fluxes from the ICOS FR-Gri station

Meteorological measurements included wind speed, air and soil temperatures and humidity as well as rainfall, global, net and photosynthetic active radiation. The vertical profile of air temperature and wind speed was measured with 5 two-dimensional ultrasonic anemometers (Wind Sonic, GILL, UK) and shielded thermocouples (HMP155, Vaisala, Finland) placed at 0.5, 1.0, 2.0, 3.0 and 5.0 m above the ground. The CO₂ and H₂O (sensible (H) and latent heat (LE)) fluxes were measured by eddy covariance with a closed-path CO₂/H₂O IRGA analyser (Li-7200, LICOR, USA) was placed at 0.2 m lateral distance from an ultrasonic anemometer (HS-50, Gill, UK). The high-frequency signals were recorded at 20 Hz by homemade Labview® program and the fluxes were computed with EddyPro (version 6.2, LICOR, USA). All flux measurements were made on a mast at 2.7 m height near the centre of the field (Fig. 1) and averaged, and standard deviations were reported over 30 minutes intervals.

295

2.4 CH₄ and H₂O mixing ratios and fluxes

CH₄ and H₂O mixing ratios were monitored using a Quantum Cascade Laser (QCL, CW-QC-TILDAS76-CS Model, Aerodyne Inc., USA) at 10 Hz. The analyser precision at one second was 2 ppb for CH₄. The analyser was sampling directly in the eddy covariance line at a flow rate of 7 NL min⁻¹ and pressure 230 mbar below atmospheric pressure. The lag time varied between 2.0 and 2.3 s for the two compounds similar to what was obtained for the PTR- Qi-TOF-MS. The QCL was calibrated prior to the experiment.

305

2.5 Footprint model and contribution of local flux to mixing ratios

The FIDES concentration and flux footprint model (Flux Interpretation by Dispersion and ExchangeS) was used to evaluate the flux footprint and to infer the contribution of the VOC fluxes to the VOC concentrations measured at the site (Carozzi et al., 2013; Loubet et al., 2018; Loubet et al., 2010). The flux footprint $\varphi(x, y)$ of the measurement mast is the probability density that the measured flux F originates from the field point of coordinates (x, y) . The measured flux is then $F = \int \varphi(x, y) f_0(x, y) dx dy$, where $f_0(x, y)$ is the surface flux at coordinates (x, y) . The flux footprint should be distinguished from concentration footprint $h(x, y)$ that relies the concentration measured at the mast C minus the background concentration C_{bgd} to the surface flux: $C - C_{bgd} =$

310

315 $\int h(x, y) f_0(x, y) dx dy$. Assuming $f_0(x, y)$ is constant over the studied field, which is a reasonable assumption for a crop, the previous equations can be integrated to provide integrated footprints:

$$F = f_0 \times \int_{field} \varphi(x, y) dx dy = f_0 \times \Phi_{field} \quad (7)$$

$$C - C_{bgd} = f_0 \times \int_{field} h(x, y) dx dy = f_0 \times H_{field} \quad (8)$$

320 Here Φ_{field} has no units while H_{field} has units of a transfer resistance ($s m^{-1}$). The model is based on the same analytical solution of the advection-diffusion equation as the Korman-Meixner model (Kormann and Meixner, 2001), All details of the model can be found in (Loubet et al., 2018).

2.6 Dataset and statistical analysis

All data were merged into a common dataset according to their date and time and averaged at hourly time steps. The dataset is available as an R format file in the supplementary material. All statistics were performed under R (R version 4.0.1, 2020-06-06).

325 3. Results

3.1 Meteorological conditions, crop development, CO₂ and energy fluxes

330 The experiment started after wheat anthesis, during the grain-filling period (Ripening stage, Figure 3). During that period, the grain was progressively filled up to reach a biomass of around 500 g DW m⁻², similar to the stems biomass (Figure 3). The senescence also started at the beginning of that period visible by an increase of the yellow-to-green leaves biomass ratio. The crop height was around 0.8-1.0 m height.

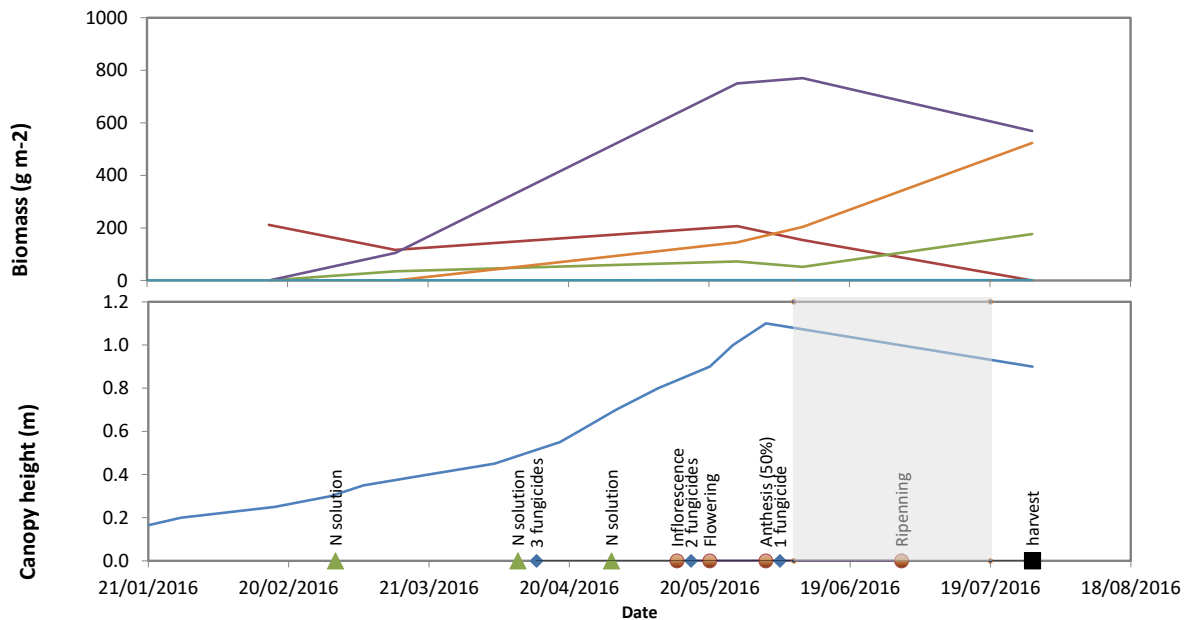


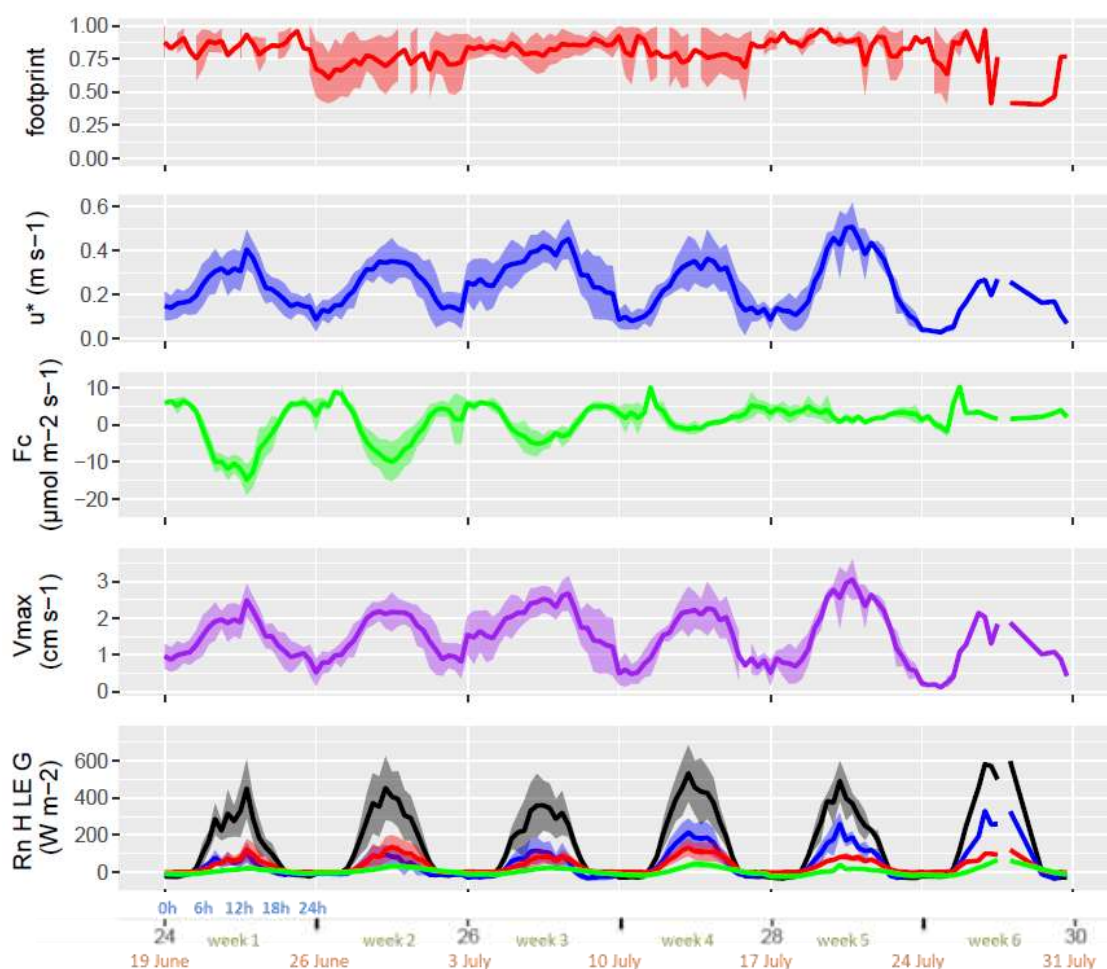
Figure 3. Top: evolution of the above ground biomass of different plant compartments. Bottom: crop height, crop developmental stages and farmer activity. The experimental period is highlighted in grey shading.

335 The campaign started a week after a major flooding event in the Parisian area characterised by a three week lasting rain period that might have affected the crop functioning. However, the CO₂ flux was in the range of expected fluxes for a wheat crop at that period. The main wind direction was west-south-west, the average wind speed

1.8 m s⁻¹ with a typical daily pattern showing night-time low wind speeds except for a few short windy periods (11-13, 20-21 and 28-31 June), accompanied by lower temperatures, higher relative humidity and consistent precipitations (**Figure S6**). Air temperature was 17.7°C on average and varied from 8 to 31°C with hot periods around 27 June, and 7 and 17 July. The period from 12 to 23 June was quite wet, while the driest periods lasted from 7 to 12 June and from 4 to 11 July. The albedo decreased slightly from 0.23 at the start of the experiment (around anthesis) to 0.18 on June 23 (grain filling period) and remained stable afterward. The air temperature at the crop roughness height z_0 (T_{z0}), which is a proxy for the plant surface temperature, varied from 10°C to 45°C.

345 The highest temperatures were observed towards the end of the campaign when at midday T_{z0} exceeded the air temperature by up to 10°C. Before that period, the air-to-canopy temperature difference did not exceed 5°C at midday. The soil temperature (measured at 5 cm depth) followed the air temperature pattern but with daytime maxima lower than air temperature by 5 to 15 degrees and night temperature slightly higher than air temperatures due to the canopy shading. The heatwave at the end of the campaign corresponded to very high water vapour pressure deficits at T_{z0} (larger than 4 kPa), while it was usually smaller than 2 kPa before. Night periods usually exhibited dew formation except towards the end of the campaign.

350



355 **Figure 4. Field flux footprint, friction velocity (u^*), CO₂ flux (F_c), maximum exchange velocity for water (V_{max}), and terms of heat balance (R_n H LE G): the net radiation (R_n , black), sensible heat flux (H, blue), latent heat flux (LE, red) and ground heat flux (G, green). By convention, except for R_n and G, positive fluxes are ecosystem losses and negative fluxes gains or up-takes. Each week shows the mean of diel cycles (lines) plus standard deviations (ribbons). The x-axis shows the week number in the year (black), the week number within the experimental period (green), the starting date of the week (orange), and the hour of day (blue).**

360 The typical friction velocity of the site was around 0.3 m s^{-1} , although it was quite high during the windy periods (2nd to the 4th week), reaching 0.5 m s^{-1} (**Figure 4**). The exchange velocity for water vapour $V_{\text{max}}(\text{H}_2\text{O})$, which is the physical limitation for convective exchanges, varied daily and showed maximum exchange rates of 3 cm s^{-1} at midday and minimum values at night near zero except during the windy periods. The CO_2 fluxes showed net absorption during daytime at the beginning of the experiment. They were fairly constant until June 15 and then
365 began to decline until July 5 (first senescence phase), when they switched to net daytime respiration (second senescence phase). Water vapour fluxes decreased less during the same period and showed a high correlation with net radiation but less to vapour pressure deficit. This indicated that although the canopy was absorbing less CO_2 , it was still transpiring, and hence the stomata were open. After week 3, the water vapour flux was rather small which indicates that at that time the crop was fully senescent and stomata were not responding to light anymore.
370 Because of the decrease of evaporation, and under quite large net radiations, the sensible heat flux increased from the 20 June onward, while the ground heat fluxes daily variations sharply increased after the 5 July. The flux footprint from the main field was mostly above 0.8 (median 0.86, interquartile 0.76 - 0.91) but showed some consistent periods with a lower footprint (down to 0.4) when the wind was blowing from the south. The periods with a footprint lower than 0.6 occupied 13% of the time.

375 **3.2 VOC mixing ratios**

The major VOCs at the site were methanol, formaldehyde, ethanol, furan, acetic acid, acetone, hydroxyacetone, acetaldehyde, isoprene and monoterpenes (**Table S3**). The mixing ratios of the most emitted and deposited VOC showed no marked daily patterns but some similarities in their weekly patterns (**Figure S7**). During the first week, mixing ratios were lower and diurnal variations smaller than during the rest of the experimental period. This weak
380 corresponded to a rainy period with westerly winds typical of oceanic influence at the site (**Figure S6**). The second week showed an increase in the mixing ratios of all compounds that mostly lasted for 3 weeks. This period corresponded to the end of the rainy period, a sudden change of the wind direction to the east and an increase in temperature and water vapour content of the atmosphere (**Figure S6**). This event also brought polluted air masses from the Parisian area as shown by the increase in NO_2 (**Figure S7**). Most compounds showed a sharp increase
385 following rain stop, and a drop after 36 weeks.

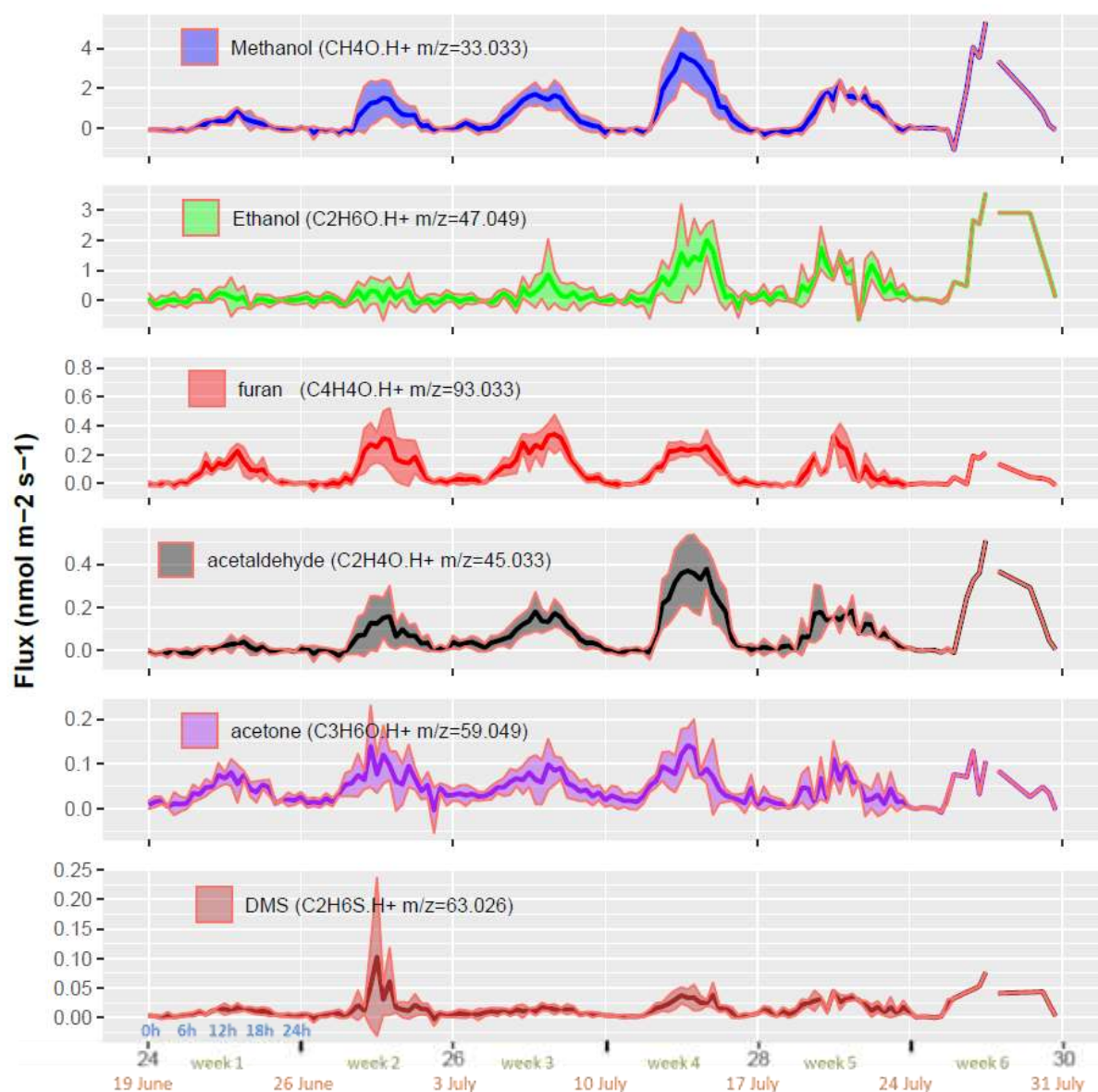
This period also showed a concentration increase of several oxygenated, mainly depositing compounds like hydroxyacetone, 4-oxopentanal, methylfuran or propyne (**Figure S7**). Week 3 corresponded to the windy period (**Figure 4**) with a well-mixed boundary layer both during day and night, and to wind blowing from the farm. The week 4 is marked by maximum concentrations of methanol and acetaldehyde but also of most of the oxygenated
390 compounds, the daily pattern of these being more marked during this week. This period, which corresponded to the end of the senescence period, was also characterised by high air temperatures (up to 30°C) and high surface temperatures (up to 40°C) (**Figure S6**), as well as by peak O_3 and NO mixing ratios, due to the first weekend of the summer holidays in France and a huge traffic rush in the region (**Figure S6**). Finally, the last week corresponded to a very warm period with low wind-speeds.

395 **3.3 VOC fluxes**

In total, 123 VOCs had fluxes greater than three times the flux detection limit (LOD_f) when computed over the whole period. However, when expressed over hourly periods, only four VOCs showed an average flux larger than

three times the mean LOD_f. This can be attributed to the fact that the LOD_f diminishes over long integration periods, because it is essentially a random error. Of these 123 VOCs, 32 were on average emitted while 91 were on average deposited.

The most emitted compound was methanol (m/z 33.033) with an average molar flux rate of 0.5 nmol m⁻² s⁻¹, which was respectively two and six times higher than the second and third most emitted VOCs ethanol (m/z 47.049) and furan (m/z 93.033) (**Figure 6, Table S3**). Acetaldehyde (m/z 45.0433) was the fourth most emitted compound, acetone (m/z 59.049) the fifth and dimethyl sulfide (DMS, m/z 63.026) the sixth. Methanol emissions increased during the first month, decreased temporarily during the 5th week to increase again during the last week of July. The daily pattern of methanol fluxes showed a sharp increase in the late morning followed by a maximum at around 12-15 h and minimum at the end of the night. Ethanol flux increased only after week 5. Furan (m/z 93.033) showed a different seasonal pattern with largest emissions during the second week, and then decreasing emissions towards the end of July, suggesting less dependency to temperature. Acetaldehyde fluxes showed a similar trend as methanol, suggesting that both are linked to a similar process. Acetone fluxes showed a rather stable daily pattern during the period, except for a slightly larger flux during week 4. DMS fluxes showed a positive peak at the end of the rain period (middle of the second week) and a decrease afterward. In addition, DMS fluxes slightly increased during the hottest period (senescence).



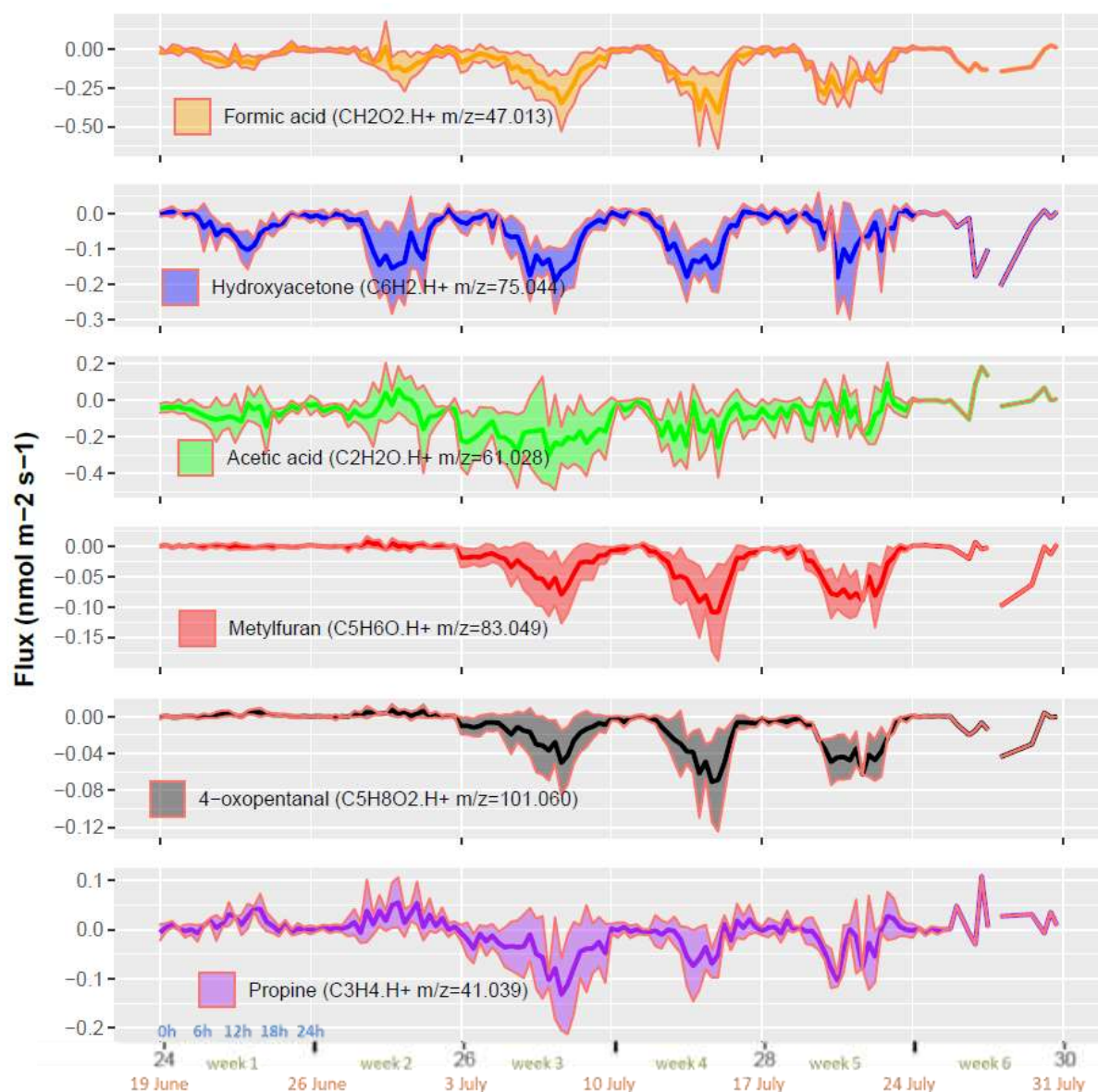
415 **Figure 6.** Whole ecosystem net fluxes of the six most emitted VOCs. Each week shows the diel cycle with its mean (line) and standard deviation (ribbons). The x-axis denotes the week number in the year (black), the week number in the experiment (green), the starting date of the week (orange), and the hour of day (blue). Note that no standard deviations are shown on week 6, because only one day of measurement was available.

420 The most net deposited VOCs were formaldehyde (m/z 31.018), formic acid (m/z 47.013), ion m/z 43.018 (which comprises fragments of several oxygenated compounds), hydroxyacetone (m/z 75.044), acetic acid (m/z 61.028), methylfuran and MBO (m/z 83.049) (**Figure 7**). These compounds contributed to 29%, 15%, 11%, 9%, 6% and 3% of the deposition fluxes summed over all compounds that passed the LOD_f criteria, on a molar basis, respectively. The VOC depositing showed distinct patterns: Formaldehyde (m/z 31.018) showed a consistently larger deposition rate during the first two weeks, followed by a decrease in deposition in the following weeks, switching to a net emission during the 5th week. Formic acid (m/z 47.013) and methylfuran/MBO (m/z 83.049) showed a small deposition during the first two weeks followed by an increase in week 3, a maximum in week 4 and a decrease during week 5. Hydroxyacetone (m/z 75.044) was deposited consistently throughout the period with larger deposition fluxes during weeks 2 to 4, mirroring the emission behaviour of furan (m/z 93.033). Ion m/z 43.018, corresponding to fragments of several ions, and acetic acid (m/z 61.028) showed a similar pattern of

425

430

bi-directional fluxes with small deposition or emission rates during the first two weeks, followed by large deposition fluxes during week 3 that decreased during the last weeks ending in small emissions.



435 **Figure 7.** Whole ecosystem fluxes of the six most deposited VOC. Each week shows the diel cycle with its mean (line) and standard deviation (ribbons). The x-axis shows the week number in the year (black), the week number in the experiment (green), the starting date of the week (orange), and the hour of day (blue). Only one day of measurement was available during week 6, leading to no interquartile computation and hence no ribbons.

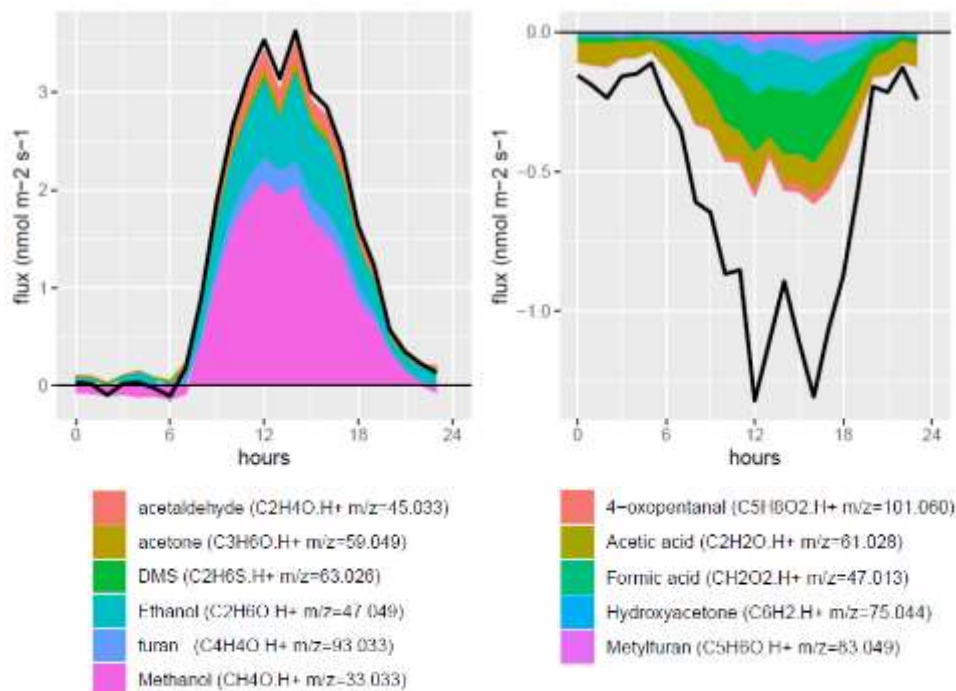
440

3.5. Total VOC emission and deposition fluxes

The sum of emissions of all VOCs was $1.02 \pm 0.04 \text{ nmol m}^{-2} \text{ s}^{-1}$ (mean \pm the sum of all LODf), which corresponds to $41 \text{ g ha}^{-1} \text{ day}^{-1}$ ($\sim 20 \text{ g C ha}^{-1} \text{ day}^{-1}$). On a molar basis, methanol contributed to 52% of the total VOC emissions, ethanol 23%, furan 9%, acetaldehyde 6%, acetone 4%, and DMS 1.3%. The average total deposition rates amounted $0.5 \pm 0.01 \text{ nmol m}^{-2} \text{ s}^{-1}$, which corresponded to $26 \text{ g ha}^{-1} \text{ day}^{-1}$ ($\sim 12 \text{ g C ha}^{-1} \text{ day}^{-1}$). Interestingly, the total VOC deposition rate was 52% of the total emission rate on a molar basis, but was around 63% when expressed on a mass basis. This shows that the deposited compounds were on average heavier than the emitted ones.

445

450 Additionally, the daily pattern of deposition fluxes showed two peaks, of which the later one coincided with the afternoon rush hour. This suggests that a great fraction of deposited VOCs stems from traffic. Indeed, parallel NO and NO₂ measurements made by Vuolo et al. (2017) showed that the site was under the advection of the roads on the north, west and east, and from the Parisian area. The first peak was rather around noon, suggesting a biological or chemical source (**Figure 8**). Overall, the summed emission and deposition fluxes led to a net flux (emission) of $\sim 15 \pm 2 \text{ g ha}^{-1} \text{ day}^{-1}$ ($0.5 \pm 0.05 \text{ nmol m}^{-2} \text{ s}^{-1}$), which approximates to $\sim 8 \pm 1 \text{ g C ha}^{-1} \text{ day}^{-1}$.



455 **Figure 8.** Stacked daily averages of the 6 most emitted (left) and 6 most deposited (right) VOCs. Black lines show summed-up emissions and depositions for compounds with fluxes larger than LODf.

4 Discussion

4.1 VOC flux eddy covariance measurements with a PTR-Qi-TOF-MS: pitfalls and open questions

460 Because of the air density fluctuations, the Webb Penman Leuning (WPL) correction needs to be applied on the eddy covariance flux (Webb et al., 1980). This correction accounts for dilution by water vapour and temperature induced density variations of the analysed air. Because of the long and heated sampling lines and large thermal mass of the drift tube, temperature variations can be neglected. Water vapour dilution however needs to be accounted for, since the water vapour fluctuations are not directly measured in the PTRMS. Eq. (S9) shows the

465 WPL correction specific to the PTR-Qi-TOF-MS. We found that this correction was most of the time smaller than a few percent (**Figure S1**), because of the relative small mixing ratios of the measured VOCs in ambient air.

Another issue that, to our knowledge, was not discussed before concerns the effect of normalising the cps by the cps of H₃O⁺ on 10 Hz data prior to calculating the eddy covariance fluxes. We showed that the bias is a function of the $\overline{w' cps'_{H_3O^+}}$ covariance, which is not null since H₃O⁺ are consumed by VOCs and water vapour that are themselves correlated to vertical wind speed (Eq. S13 and S14). However, this bias is small and negligible when integrated over time (**Figure S2 and S3**). Nevertheless, we recommend to calculate the covariances using raw cps

and normalise them by the primary ion H_3O^+ afterwards, to avoid this minimal though proven bias. This is important especially in conditions with very strong fluxes since $\overline{w' \text{ cps}'_{\text{H}_3\text{O}^+}}$ may increase under such conditions.

475 High frequency losses were evaluated to be small and in line with the expected values for the lag time of our sampling system (lower than 5%) (Ammann et al., 2006). These high frequency losses were estimated from the first water cluster (m/z 37.028, **Figure S5**). Based on the comparison of the shapes of the cross-correlation functions for the water cluster and methanol (**Figure S4**), we hypothesise that the high frequency losses for methanol should be similar to that for water vapour. Since methanol is a sticky compound, we expect that this would be also true for most measured VOC. However, we were unable to evaluate high-frequency losses for
480 methanol based on its *w.cps* cross-spectra, which showed higher values at high frequencies than at lower ones (**Figure S5**). We interpret this as an effect of the noise-to-signal ratio of the VOC cps (Langford et al., 2015). Although we expected some large noise contribution to the variance of the VOC signals, we did not expect a contribution to the *w.cps* cross-spectra. The cross-spectra exemplified in **Figure S5** however shows the opposite. A reconstruction of the a noisy signal mimicking that of methanol (not shown) confirms that noisy signals are
485 difficult to analyse for high frequency losses since the high frequency end of the signal is dominated by the noise. To tackle this issue, one would need to develop some denoising algorithm, which is beyond the scope of this manuscript.

4.2 Magnitude of major VOCs exchanged

Overall, we were able to identify more than 123 VOCs that had fluxes larger than three times the flux limit of detection (LOD_f). Park et al. (2013a) reported almost 500 VOCs whose fluxes exceeded three times the LOD_f. This is not fully surprising, that we found less VOCs showing a significant flux, since Park et al. measured above an orange orchard in the Central Valley of California in the summer, which is a much more emitting ecosystem in a much period favourable to emissions (Park et al., 2013b). Indeed, they found a methanol flux ($73 \mu\text{g C m}^{-2} \text{ h}^{-1}$) around three times larger than in this study ($23 \mu\text{g C m}^{-2} \text{ h}^{-1}$), and similarly for acetone and acetaldehyde. Overall,
495 their fluxes were hence at least three times larger than ours, which probably explains the larger number of compounds having a flux above the LOD_f in their study. Interestingly however we found around the same number of depositing compounds (~190) (Park et al., 2013a). Note that although the most deposited compound was formaldehyde, it is not discussed here since the uncertainties in its concentration measurement, especially in response to water vapour are too large in this study to provide consistent measurements.

500

In our study **Methanol (m/z 33.033) was by far the most emitted VOC**. Jacob et al. (2005) estimated that growing vegetation is the major source of methanol at the global scale (128 Tg yr^{-1}) followed by recombination of methylperoxyradicals (CH_3O_2) with itself and other organic peroxy radicals (38 Tg yr^{-1}), plant decay (23 Tg yr^{-1}), biomass burning and biofuels (13 Tg yr^{-1}), and vehicles and industry (4 Tg yr^{-1}). The very few studies on VOC fluxes from wheat (**Table 1**), reported that methanol is the most emitted compound representing 20 to 80% of the overall VOC fluxes (Bachy et al., 2020; Gonzaga Gomez et al., 2019). Hence, our results corroborate these previous studies suggesting that cereal crops represent a potential strong source of methanol, at least for winter
505 wheat in Europe.
510

More specifically, our study confirms the increase of methanol emissions during senescence (**Figure 6**) as already observed by Bachy et al. (2020) and Gonzaga et al. (2021) on wheat and Mozaffar et al. (2018) on maize. These observations collectively suggest that cereal crops become a major source of methanol at the end of cultural cycle with net emission rates possibly exceeding those during the vegetative growth phase. This seasonal peak can be explained by the demethylation of pectin in senescent plant tissues (Michele et al., 1995) along with the pronounced degradation of cellular components at the end of chlorosis (Keskitalo et al., 2005; Woo et al., 2019), both of which promote methanol production and its release through higher leaf porosity. In addition, methanol emissions were enhanced by high tissue temperatures during the senescence period due to warm weather conditions and reduced transpiration (**Figure S6 and Figure 6**).

We recorded rather small deposition rates at the end of the night, when the canopy was the wettest (**Figure 6**). As a very soluble compound, methanol can be easily adsorbed in water layers and desorbed when the canopy dries out (Bachy et al., 2018; Laffineur et al., 2012). However, we did not find any clear desorption pattern in the morning, suggesting rather moderate net surface deposition at night in our study.

Ethanol (C₂H₆O, m/z 47.028) is an intermediate in the production of acetaldehyde under anoxic conditions in the root system by fermentation. After transport to the leaf level, ethanol is oxidised to acetaldehyde, which can be further oxidized into acetate (Kreuzwieser et al., 2001; Niinemets et al., 2014; Seco et al., 2007). Indeed in our study, ethanol and acetaldehyde emissions expressed a similar pattern suggesting that the two compounds originate from closely associated processes, which is in line with the MEGAN model, which assigns the same emission factor to ethanol and acetaldehyde (Guenther et al., 2012). Ethanol was also identified as a dominant VOC emitted by corn silage due to fermentation, making up typically 3% of the VOC US emissions (Hafner et al., 2010; Montes et al., 2010).

Furan emissions from crops (tentative identification of m/z 93.033) were not reported in previous studies so far, apart from the work of Gonzaga et al. (2019) using plant chambers with the same instrument at the same site (**Table 1**). In their study they observed maximum fluxes during the grain-filling period (**Figure 4**). To our knowledge, the only other studies reporting emissions of this compound are those by Stockwell et al. (2016) from biomass burning, Venneman et al. (2020) from root endophytic fungi (*Serendipita*), and Park et al. (2013b) from an orange orchard. Park et al. (2013b) reported an average flux of 4.2 $\mu\text{g C m}^{-2} \text{h}^{-1}$ over 24h, which is about 5 times lower than what we observed here, suggesting that this compound may be specific to wheat (**Table 1**). Other studies mentioned furan but either identified as a compound emitted from the chamber material or a compound which flux remained below the detection limit (Batten et al., 1995; Gitelson et al., 2003). In our study, because of the method used to measure the flux, a desorption process from the tubing is not plausible. Indeed, this would mean that desorption would be correlated with vertical wind speed at high frequency, which is not likely.

Acetaldehyde (m/z 45.033) was the third most emitted compound with a flux range similar to that reported in previous studies on wheat (**Table 1**). The measurements from Gonzaga et al. (2019) with dynamic chambers shows remarkable agreement during the same grain filling period, suggesting the plant is the main source at that time. Bachy et al. (Bachy et al., 2020) determined significantly lower average values, which is explained by the fact that their values refer to the entire season, whereas our values refer to the grain filling period. The emission pattern of

acetaldehyde was very similar to that of methanol, suggesting a similar production process leading to emissions, or at least a similar dependency of these processes to environmental conditions and plant and soil physiology (**Figure 4 and 6**). However, the mechanisms leading to acetaldehyde emissions are not well characterised yet, especially in the field. Enhanced acetaldehyde emissions were observed following leaf wounding (De Gouw et al., 2000; Graus et al., 2011), light-dark transition (Karl et al., 2002) and exposure to oxidative (ozone) and anoxic stresses (Seco et al., 2007). The latest observation may be particularly relevant for the present study, since the wheat crops at our site are frequently exposed to high ozone deposition fluxes and thus oxidative stress (Potier et al., 2015; Stella et al., 2013; Tuzet et al., 2011; Vlasenko et al., 2010). Potier et al. (2017) have shown that ozone reacts strongly with wheat leaf water extracts and especially when wheat is senescent. Moreover, water treatment ozonation studies have shown that organic matter oxidation is a source of acetaldehyde (Papageorgiou et al., 2014). These studies altogether suggest that acetaldehyde emission from crops through oxidation of organic plant or soil material by ozone may be a significant emission source. This source would especially be significant during senescence when the cells degrade and organic matter is exposed to the atmosphere. This hypothesis is supported by the work from Potier et al. (2017; 2015), showing an increased ozone deposition during senescence over wheat.

Globally, In our study, **acetone (m/z 59.049)** was among the most emitted compound, similarly to what Bachy et al. (2020) and Gonzaga et al. (2019) over wheat. Acetone is known to be mostly emitted by terrestrial vegetation (~30% of the total emissions) and oceans (~30%), with additional sources being plant decay (2-10%) and oxidation of isoalkanes in the atmosphere (Jacob et al., 2005). Maillard reactions in dead decaying plant material was identified as a potential important source of acetone (Warneke et al., 1999). Increased acetone emissions from intact plants were observed upon stresses including injury (Davison et al., 2008), ozone exposure and water logging (Cojocariu et al., 2005). Fruekilde et al. (1998) suggested that acetone is produced at the plant surfaces from the ozonolysis of epicuticular waxes. The available literature therefore suggests that acetone emissions by plants may significantly come from non-enzymatic reactions occurring during degradation of plant cells and surfaces. Soil may be an additional source of acetone, increasing with soil organic matter (Abis et al., 2018; Schade and Goldstein, 2001; Zhao et al., 2016). In particular, acetone was proved to be a secondary product of the cyanogenic pathway (Seco et al., 2007).

Table 1. Fluxes and mixing ratios of the 10 most emitted VOC found in this study, together with isoprene and monoterpenes, compared to literature values using different methods of measurement. VOC fluxes measured by eddy covariance refer to the whole ecosystem including soil and are expressed per m² of ground surface. Fluxes from chamber measurements refer to projected surface and dry weight of the enclosed aboveground organ of wheat. Means ± standard errors and [min – max] ranges.

m/z	Tentative identification	Mixing ratio ppb	Flux		Measurement method	Reference	
			µg m ⁻² h ⁻¹	ng g ⁻¹ DW h ⁻¹			
33.033	Methanol	3.4	63 ± 4	30 ± 2	Eddy cov.	this study	
			[1 – 10]	62 ± 3.3	[680 – 1100]	Dyn. Chamb.	G2019
47.049	Ethanol	1.7	41 ± 4	20 ± 2	Eddy cov.	this study	
93.033	Furan (C ₆ H ₄ O)	1.7	30 ± 1.5	15 ± 1	Eddy cov.	this study	
			[10 – 50]			Dyn. Chamb.	G2019
45.033	Acetaldehyde	0.3	9.6 ± 0.6	5 ± 0.4	Eddy cov.	this study	
					[10 – 50]	Dyn. Chamb.	G2019
59.049	Acetone	0.7	9.1 ± 0.3	4.5 ± 0.15	Eddy cov.	this study	
					[80 – 180]	Dyn. Chamb.	G2019
63.026	DMS	0.1	2.9 ± 0.15	1.5 ± 0.1	Eddy cov.	this study	
			[0 – 11.6]		[0 – 14.5]	Static chamber	K1995
			[0.2 – 0.5]	0.03	Dyn. chamber	F1988	
95.049	Phenols	0.1	3.2 ± 0.3	1.6 ± 0.1	Eddy cov.	this study	
69.070	Isoprene + fragments	0.2	-1.3 ± 0.2	-0.6 ± 0.1	Eddy cov.	this study	
			4.8	[0 – 6000]	Dyn. Chamb.	M2016	
			[-10 – 25*]	[-5.5 – 14]	Eddy cov.	B2020	
				[0 – 50]	Dyn. Chamb.	K2009	
137.132	Monoterpenes	0.2	-2.6 ± 0.1	-1.3 ± 0.05	Eddy cov.	this study	
					[-50 – 18]	Dyn. Chamb.	G2019
			[0 – 12 000]		[0 – 420 000]	Dyn. Chamb.	M2016
			[-10 – 25*]	[-5.5 – 14]	Eddy cov.	B2020	

F1988 (Fall et al., 1988). K1995 (Kanda et al., 1995). K1995 (Konig et al., 1995). K2009 (Karl et al., 2009a). B2020 (Bachy et al., 2020). G2019: (Gonzaga Gomez et al., 2019). M2016 (Morrison et al., 2016). In this study, 18 T ha⁻¹ dry biomass, which is the mature wheat field biomass, was used as a scaling parameter. K1995: closed chamber measurements were performed over 10 minutes twice a day in PVC chambers. * Rough estimations based on averaged diurnal cycles. # m/z 68.06 which C₅H₈+ is used as proxy. It is multiplied by 12 to 24, which is the slope of m/z69.07 to m/z68.06 at E/N=150 and E/N=130 respectively.

590

To date **Dimethyl sulphide emissions (DMS, m/z 63.026)** from terrestrial plants have been rarely reported. The fluxes DMS observed in our study are in very good agreement with those from Kanda et al. (1995) who measured DMS emissions from maize and wheat with static chambers, a technique which may however be criticised for exposing the plants to unnatural, non-steady state environmental conditions (Niinemets et al., 2011). Kanda et al. (1995) however, clearly showed that the above ground part of the wheat was the source. Yonemura et al. (2005) found emissions from *Hibiscus spec.* in quantities comparable to our studies (~6 µg m⁻² h⁻¹). whereas Vettikkat et al. (2020) reported large emissions of DMS by tropical forest trees (Mahogany tree, *Swietenia macrophylla*) in the range of 7-40 µg m⁻² h⁻¹ (assuming a LAI of ~7 m² m⁻² as observed in the present study).

595

Jardine et al. (2015) reported large DMS concentrations in the Amazon forest, and showed that a soil source was present. Globally, the largest identified DMS sources so far are oceans (~100 times larger than terrestrial source), through the dimethylsulphoniopropionate (DMSP) production by phytoplankton in their photosynthetic cycle (Groene, 1995). Interestingly, DMSP was also found to be emitted from several terrestrial species, and to increase under drought stress (Haworth et al., 2017). In our study we noticeably found larger DMS emissions during the second week (**Figure 6**), which corresponded to a period with a consistently larger atmospheric water vapour concentration and some rain. This suggests that DMS emissions from wheat are promoted by wet conditions. However, Gonzaga-Gomez et al. (2019) did not find DMS to be emitted by wheat leaves in amounts similar to our study, suggesting an emission rather from the soil during that period. Carrión (2017) suggested soil DMS emissions from methanethiol degradation by soil bacteria. Indeed, Abis et al. (2018) found emissions from sieved soils, though small in magnitude. Furthermore, Venneman et al. (2020) showed clear emissions of DMS from root endophytic *Serendipita* fungi. Clearly, DMS emissions by terrestrial ecosystems, and soils in particular need further investigations.

Isoprene (m/z 69.070). Crops are generally considered as low emitters of isoprene (Lathière et al., 2010). Indeed in our study, isoprene was mostly depositing, except during the first week (**Figure 6**). Bachy et al. (2020) also reported deposition events, especially during senescence in the early morning. Since isoprene is fragmenting and other compounds fragment on m/z 69.070, the observed deposition of m/z 69.070 may include other compounds than isoprene (Karl et al., 2012; Zhou et al., 2017). This issue is discussed in the supplementary material (**Figure S11**). Especially, we see that ion $C_5H_8^+$ (m/z 68.050) that corresponds to the that Assuming that ion $C_5H_8^+$ (m/z 68.050) is a proxy of isoprene, this ion mostly showed emissions except for week 28, suggesting that isoprene may be emitted by wheat, but MBO and other fragmenting compounds would be mostly depositing. Bearing in mind that it is a hypothesis, we conclude that isoprene was mostly emitted at a rate close to Morisson et al. (2016) and similar to Bachy et al. (2020) (**Table 1**).

Monoterpenes (MT, m/z 137.129) were mostly depositing (**Table 2**), with a flux range similar to that of Bachy et al. (2020). We found that the cps of ions m/z 81.070 and 137.129 were highly correlated (correlation coefficient = 0.98), with a ratio 81/137 of 2.5 (**Table S4**), in agreement with previous studies (Misztal et al., 2012; Steeghs et al., 2007; Tani et al., 2004; Tani et al., 2003). This ratio and the correlation coefficient were stable whatever the E/N, though slightly higher at E/N = 150 (2.7). However, interestingly the m/z 137.129 deposition flux was larger than that of m/z 81.070, while the mixing ratios were ranked in an opposite way. This indicates that the monoterpenes were composed of a mix of compounds having different deposition velocities and different fragmentation patterns. Indeed the ratio of m/z 81/137 was shown to depend on the monoterpene compound and E/N (Misztal et al., 2012). According to their study, and bearing in mind the many uncertainties, the measured ratio 81/137 in our study would correspond to 3-carene. Deposition of monoterpenes was observed over grassland by (Bamberger et al., 2011) during an episode when the surrounding pine forest was damaged by a hailstorm, hence showing that monoterpenes can be deposited when ambient concentration is large. In our study, the wheat field was next to a woodland and farm, both being a source of monoterpenes (Kammer et al., 2020), that clearly enhanced the mixing ratios of MT under favourable wind conditions. (**Figure S13**). This suggests that the MT deposition was governed by local advection from surrounding sources. Deposition of monoterpenes was also

demonstrated by modelling studies even for low MT emitting canopies, confirming a bi-directional behaviour of
640 MT fluxes (Zhou et al., 2017).

Phenols (m/z 95.049). Phenol emissions from terrestrial surfaces are mostly due to biomass burning but also to
fresh manure and livestock (Kammer et al., 2020). Phenol is common in decomposing organic material. However,
we found no literature data on phenol emissions from plants or soils. Our experimental field receives a lot of
645 manure and slurry (Loubet et al., 2011), which together with the organic matter of senescing plants may have
mostly contributed to the overall phenol emissions. Phenolic compounds, and especially phenol-propanoids and
benzenoids is a class present in all plants and essentially produced via the shikimate pathways from amino acids
(Fares et al., 2010), and in wheat noticeably (Király, 1962).

650 Formic acid (CH_2O_2 , m/z 47.013) was the second most depositing VOC, which also had high deposition
velocities. Link et al. (2020) showed that it is formed from the oxidation of isoprene degradation products (MACR,
isoprene epoxydiol, IEPOX, isoprene hydroxy hydroperoxide, ISOPOOH) with the OH radical. The daily pattern
of V_{dep} showed clear deposition during the day, and the smallest deposition rate at the end of the night. Formic acid
is also known to be produced by organic matter degradation (Holopainen et al., 2017), and several studies observed
655 clear emissions of formic acid from ecosystems (Nguyen et al., 2015; Rantala et al., 2015). Bi-directional fluxes
were indeed reported by Brillì et al. (2016) in a European forest, and by Jardine et al. (2011) in a tropical forest,
who estimated the compensation point being around 1.3 ppb. In our study, we had however smaller atmospheric
concentrations suggesting that the compensation point was much smaller (lower than 70 ppt).

660 **The third most deposited ion was $\text{C}_2\text{H}_2\text{O}$ (m/z 43.018, Table 2).** Although the raw formula of this ion is quite
clear ($\text{C}_2\text{H}_2\text{O.H}^+$) and would correspond to ethenone, it is most certainly a mix of several fragments (2,3
butanedione, acrylic acid, methyl vinyl ketone, acetic acid, formic acid), as shown by the synthesis of Yáñez-
Serrano (2021)). In particular, it was shown to be a fragment of acetic acid (Baasandorj et al., 2015). We indeed
found a correlation of 0.9 between m/z 61.028 and m/z 43.018 mixing ratios and also observed between the two
665 ion fluxes (**Figure 7**). We also found a correlation of 0.84 between m/z 71.049 (MVK and MACR) and m/z 43.018
cps. Ion m/z 43.018 deposition velocity did not show a very clear diurnal pattern. However, during the stormy
week (week 3), the deposition flux and velocity increased in magnitude (**Figure 7 and 9**). The absence of clear
daily pattern in deposition velocity is surprising since V_{max} itself shows a diel pattern. This may be related to a
surface resistance that compensates the daily variations in V_{max} , namely higher surface resistance during the day
670 and lower ones at nights due to the affinity with water of these compounds that are mostly polar. Indeed, at night
leaf surfaces were often wet while they were dry during the day, as shown by the wetness index (**Figure S6**). Ion
m/z 43.018 was also emitted during a short dry period at the start of the senescence, but no emissions, nor strong
deposition were observed when the canopy was either growing or completely senescent. This bi-directional
behaviour may be due to the fact that this ion is a combination of several compounds.

675 **Hydroxyacetone** was the fourth most depositing compound (m/z 75.044, $\text{C}_3\text{H}_6\text{O}_2$, **Table 2**). Hydroxyacetone
(HAC) is an oxidation product of isoprene after oxidation by O_3 , OH or NO. High deposition velocities above a
forest averaging 1.4 cm s^{-1} have been reported by Nguyen et al. (2015). In our study deposition velocity of HAC

was about 20 times lower, which can be partly explained by the lower turbulence level above a wheat crop with respect to a forest canopy, leading to higher transfer resistances (Seinfeld and Pandis, 1998). We estimate that in our study the maximum exchange velocity (V_{\max}), which expresses the maximum deposition velocity for a non-reactive compound, was 3 to 4 times lower than in Nguyen et al. (2015). We are not aware of other studies reporting hydroxyacetone deposition over crops. In terms of carbon, HAC deposition represented about 1/3 of the methanol emission and was 3 times the isoprene emissions (**Table 1**). Regarding its diurnal variation, the deposition velocity showed a very clear pattern with an increase early in the morning, a quite constant V_d throughout the day, and a decrease late in the evening (**Figure 9**). Nguyen et al. (2015) found a similar increase in the morning but a decrease that started earlier during the day and became enhanced towards the evening. The difference between these studies may suggest a difference in the non-stomatal deposition or in the daily turbulence pattern between studies. Products of atmospheric VOC oxidation like HAC can be taken up by plants and metabolized as shown for example by Karl et al. (2010).

Table 2. Fluxes and mixing ratios of the six most depositing VOCs¹ found in this study, compared to measurements reported in the literature over any type of vegetation.

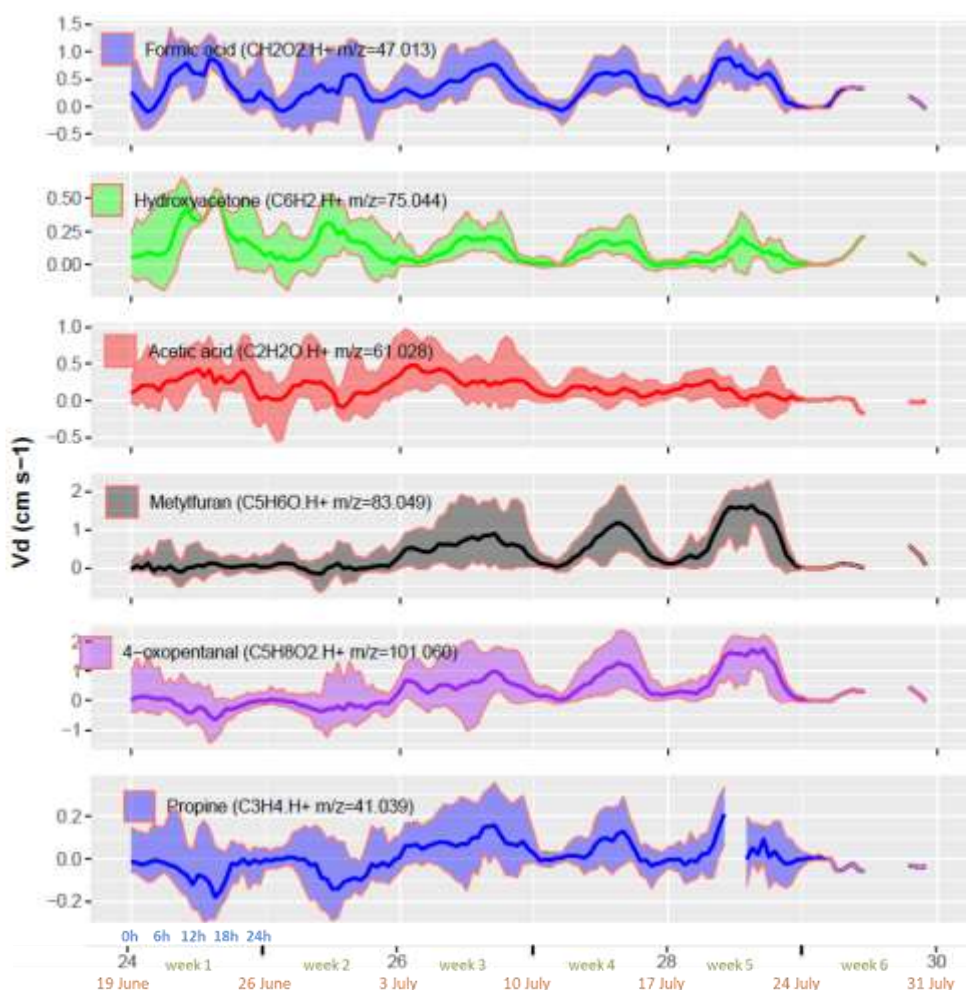
m/z	Tentative Raw formula	Tentative identification	Mixing ratio ppt	Flux nmol m ⁻² s ⁻¹	Vdep mm s ⁻¹	Reference
75.044	C3H6O2	Hydroxyacetone (HAC)	510 [2 – 1200] [50 – 1300]	-0.05 [-0.2 – 0.02] -0.2 [-0.6 – 0.05]	-0.1 [-0.6 – 0.3] 1.4 ± 0.5 [0 – 2]	This study N2015
43.018	C2H2O	Fragments ¹ Ethenone	510 [50 – 1240]	-0.05 [-0.21 – 0.06]	0.1 [-0.1 – 0.5]	This study
61.028	C2H4O2	Acetic acid	220 [0 – 550]	-0.03 [-0.13 – 0.03]	0.2 [-0.2 – 0.7]	This study R2011
83.049	C5H6O	Methylfuran	40 [9 – 90]	-0.02 [-0.10 – 0.01]	-0.03 [-0.7 – 0.5]	This study
47.013	CH2O2	Formic acid	270 [0.8 – 740]	-0.08 [-0.3 – 0.02]	0.3 [-0.2 – 1.0]	This study
101.059	C5H8O2	4-oxopentanal Pentenoic acid	20 [3 – 50]	-0.01 [-0.06 – 0.01]	0.3 [-0.6 – 1.7]	This study R2011

¹ formaldehyde was the most depositing compound measured. However because of the uncertainties linked with its response to water vapour, fluxes are not reported here. See Yáñez-Serrano (2021). N2015: (Nguyen et al., 2015). Ranges were estimated from **Figure S17**. R2011: Ruuskanen et al. (2011). Values in brackets are min and max. K1998: Kesselmeier et al. (1998). Fluxes were measured over barley and expressed per leaf area index. They were multiplied by the maximum are index observed in this study (7 m² m⁻²), to transform to comparable units. Value under brackets are standard deviations

The fifth most depositing compound was acetic acid (m/z 61.028). Acetic acid is formed in the atmosphere by oxidation of isoprene, and its oxidation products, with O₃ and OH at low NO (Link et al., 2020). Acetic acid can also be directly emitted from soils (Mielnik et al., 2018), and from plants especially under stress conditions and during senescence (Portillo-Estrada et al., 2020). Kesselmeier et al. (1998) found emissions of acetic acid from trees but only deposition on barley and other crops, suggesting a bi-directional stomatal uptake and subsequent usage by plant metabolism, confirmed by Staudt et al. (2000). In the present study, acetic acid deposition velocity did not show a clear diurnal pattern though V_d was slightly larger in the morning than in the afternoon (**Figure 9**). This behaviour may reflect the presence of dew in the wheat canopy and at the soil surface during the morning, where acetic acid would be efficiently trapped. It may also be due to an afternoon source of acetic acid from the plant metabolism or soil that would partially compensate its deposition. Acid emission was indeed shown to increase with temperature (Filella et al., 2007) and transpiration (Kesselmeier et al., 1998). The diurnal mechanism

of turgor regulation could also influence the net-acid exchanges by plants. During the day the pH level in the apoplasm are reduced, which increases the gaseous to aqueous ratio of acids, and hence their volatilisation (Gabriel et al., 1999).

715 **Methylfuran (m/z 83.049, C₅H₆O)** was the sixth most depositing compound. It also had one of the highest deposition velocity in our study. Little can be found in the literature about fluxes of this compound, but is a very well-known oxidation product of isoprene (Karl et al., 2009b). Helmig et al. (1998) reported Methylfuran mixing ratios of 90 ppt near the ground and 80 ppt throughout the whole boundary layer over a tropical forest, suggesting a near-ground source in this environment. Methylfuran is known to be formed primarily during combustion processes, and is commonly detected in biomass burning plumes (Hatch et al., 2017; Koss et al., 2018). In this study the deposition velocity showed a marked diurnal cycle with a maximum around 14h and a minimum at night (**Figure 9**). From week 3, a sharp increase in m/z 83.049 deposition velocity was observed coinciding with the onset of senescence, as seen by the decrease in the net photosynthesis (**Figure 4**). Diurnal and seasonal patterns were similar between m/z 83.049 and m/z 47.013 (formic acid) after week 3, suggesting a similar deposition process for the two ions during senescence (**Figures 7 and 9**). Although unlikely, a possible change in the fragmentation patterns may also have contributed to the increase of methylfuran deposition in week 3.



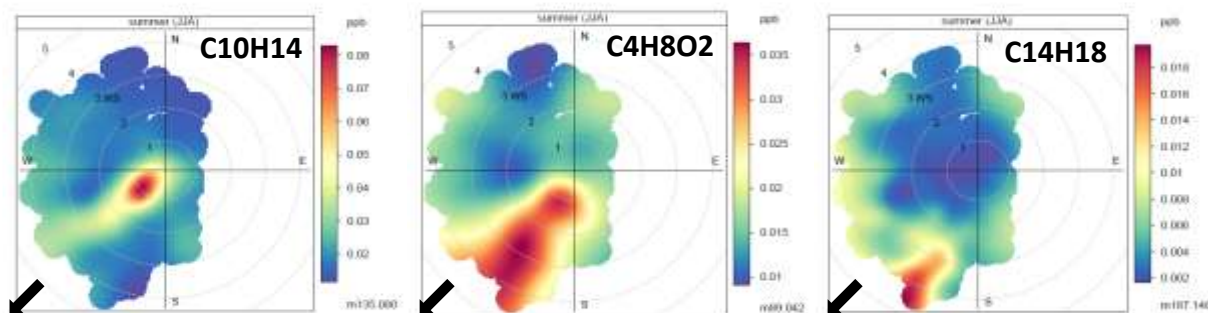
730 **Figure 7. Diurnal cycle of deposition velocity of the six most depositing VOC. Each week shows the diel cycle with its mean (line) and standard deviation (ribbons). The x-axis shows the week number in the year (black), the week number**

in the experiment (green), the starting date of the week (orange), and the hour of day (blue). Only one day of measurement was available during week 6, leading to no interquartile computation and hence no ribbons.

735 **4-oxopentanal (4-OPA, C₅H₈O₂, m/z 101.059)**, also possibly pentenoic acid, was reported to be emitted by pig slurry (Feilberg et al., 2015; Ni et al., 2012) as well as from cow and sheep farms (Hobbs et al., 2004; Kammer et al., 2020), but no deposition was reported previously to our knowledge. Pentenoic acid is also known to play a role in bacteria-fungi interactions in soil (Effmert et al., 2012; Scholler et al., 2002). Jud et al. (2016) observed 4-OPA formation from ozonolysis of plant essential oils or diterpenes present on plant surfaces. Similarly, ozonolysis of squalene, a triterpene present in all plants was reported to produce 4-OPA (Xiong et al., 2019). In this study, 740 C₅H₈O₂ was behaving very similarly to methylfuran (C₅H₈O). Indeed, their mixing ratios had a correlation coefficient of 0.95, and both showed similar deposition velocity patterns with an increase from week 3 onwards, suggesting that the deposition of these compounds was promoted during senescence.

4.4 VOC mixing ratios influenced by the nearby farm

745 Since many volatile organic compounds were bidirectionally exchanged, the question arises whether the observed mixing ratios correspond to those of the suburban region or were largely influenced by the local environment, especially the nearby farm with livestock and the surrounding fields. By analysing the mixing ratio frequency as a function of the wind direction and wind speed, several compounds were clearly identified as coming from the nearby animal farm (Figure 10, Figure S12-S14, and Table S3). Some of these VOCs are directly emitted by the farm Kammer et al. (2020), namely acetic acid (m/z 61.028), monoterpenes (m/z 137.129 and its fragment m/z 750 81.070), as well as m/z 136.000, identified as a Benzothiazole (C₇H₅N₃). The pollution rose of these compounds showed three typical behaviours (Figure 10).



755 **Figure 10.** Three typical wind rose of compounds identified as coming from the farm. Colours show the mixing ratios, and plots are binned by averaged wind direction and wind speeds. Left: constantly emitting source (example C₁₀H₁₄). Middle: source emitting with a daily pattern (example C₄H₈O₂). Right: secondary photo-produced compound (example C₁₄H₁₈). The arrow indicate the direction of the main farm buildings.

760 The VOC m/z 135.117 (identified as C₁₀H₁₄, para-cymene) showed large mixing ratios for a narrow wind sector and low wind speed similar to the methane pollution rose (Figure S12), which is a tracer of the livestock. The observed diel variation in mixing ratios is typical for a local source that is emitting constantly during the day and night. Indeed, turbulent mixing and hence dilution was higher during the day than at night (Figure S6). Compounds that behaved similarly were monoterpenes (m/z 137.129), and an oxygenated monoterpene (m/z 153.127) (Figure S13).

By contrast, the VOC m/z 89.042 ($C_4H_8O_2$) showed high mixing ratios for a larger wind sector and for both low and high wind speeds. This is a less usual behaviour, which may reflect the fact that emissions concomitantly increase with wind speed, hence compensating the turbulent mixing effect. Since wind speed and temperature are correlated with each other throughout the day (**Figure S6**), we hypothesize that emissions of this compound increased with temperature of the source inside the farm, which is influenced by the temperature outside. Indeed the mixing ratios for this compound scaled positively with air temperature (**Figure S13**). VOCs behaving similarly were acetic acid (m/z 61.028), m/z 103.075 ($C_5H_{10}O_2$) and m/z 117.084 ($C_6H_{12}O_2$). Kammer et al. (2020) found that all these compounds originate from the stable and are associated with silage feeding. Silage is indeed a source of these compounds as well as ethanol, linked to microorganism's activity which increase with temperature. Finally, VOCs m/z 187.148 ($C_{14}H_{18}$ or $C_{11}H_{22}O$) showed large mixing ratios for a narrow wind sector and only for wind speeds larger than $\sim 3 \text{ m s}^{-1}$. Since these wind speeds occurred only in the middle of the day at that site (**Figure S6**), we hypothesize that during its travel from the farm these compounds were either rapidly broken down and removed from the air, and/or were secondary produced from other primary emitted VOCs by photochemical reactions. Using the 3 m s^{-1} threshold observed in **Figure 10**, we infer a travel time of ~ 2.5 min. Alternatively, these VOCs were transported from an incinerator 2 km away, which was identified as an SO_2 source (Loubet et al., 2012). This incinerator, which can emit both day and night is however a bit more west than the farm (225 deg/N). Therefore, the source of the VOCs representing m/z 187.148 may rather be the farm. Compounds that behaved similarly were heavy ions (m/z 201.139, and m/z 201.233) indicating oxidised VOCs.

5. Conclusions

We found that the PTR-Qi-TOF-MS was sensitive enough to measure fluxes of 264 VOCs by eddy covariance (77 emitting and 187 depositing, fluxes $> 3 \text{ LODf}$) above a wheat canopy during the ripening and senescence periods. The fact that fewer compounds were net emitted than net deposited can be explained by the higher atmospheric mixing ratios of the depositing compounds, compared to the emitting ones. In particular, the nearby farm contributed to increasing the ambient concentration of some VOCs, most of which quite heavy, including monoterpenes, but also more light VOCs like acetic acid.

Detailed analysis of the eddy covariance flux computation revealed that the Webb Penman Leuning (WPL) correction was negligible (most of the time lower than 2%). Similarly, normalising by the H_3O^+ cps at high frequency was shown to produce mostly negligible biases. Based on water vapour cluster, we found a small high-frequency loss in our setup. However, found difficult analysing the high-frequency response of the noisy signals of most VOCs, including methanol. Further analysis of the high-frequency losses with a PTR-TOF-MS is still required to better characterise these potential errors.

Our measurements confirm previous findings showing that methanol is the most emitted compound from wheat fields, representing 52% of the total VOC moles emitted by the crop. Acetone and acetaldehyde were also found to contribute significantly to the summed VOC emissions. However, we detected several other compounds not previously reported as emitted by wheat. In particular, furan (m/z 93.033), which may be released by decomposing organic matter. Moreover, substantial DMS emissions were measured which confirms earlier findings on the magnitude of the terrestrial DMS source and suggest that soils may be a significant source of DMS together with plants and litter. Furthermore, we found large deposition rates of oxygenated VOCs, in particular formic and acetic acids together with hydroxyacetone and 4-oxopentanal. The deposition of many VOCs was enhanced during

senescence, suggesting either an uptake process or a gas phase interaction with compounds emitted by the plant at that stage. These putative processes would need further investigations.

805 It is the first time 123 VOCs fluxes (above 3 LOD) measured by eddy covariance are reported over a wheat field. Overall, the summed VOCs emissions amounted $41 \text{ g ha}^{-1} \text{ day}^{-1}$ and summed deposition amounted $-26 \text{ g ha}^{-1} \text{ day}^{-1}$, leading to a net flux of $\sim 15 \text{ g ha}^{-1} \text{ day}^{-1}$. When roughly extrapolated to the whole year, the summed VOCs flux amounted around $3 \text{ kg C ha}^{-1} \text{ year}^{-1}$, an amount negligible compared to the CO_2 flux ($17 \text{ Mg C ha}^{-1} \text{ year}^{-1}$). Our study confirms that the most emitted compound from wheat has a low reactivity (methanol). It however highlights
810 that wheat is an active sink for a number of oxygenated compounds.

Using a PTR-Qi-TOF-MS to measure VOC fluxes over an ecosystem for a long period by eddy covariance allows estimating the fluxes of a large number of compounds and establishing a net flux. The main difficulty remains the clear identification of the compounds corresponding to each ion, as well as the calibration of a large number of gases.

815 **Code availability**

The Labview code to record the data is available on demand, and the R code used to compute the fluxes is on the following repository: <https://forgemia.inra.fr/Benjamin.Loubet/cov3er>

Data availability

820 The complete hourly dataset is available as an Rdata file (*COV3ER_2016_dataset.Rdata*) containing the whole dataset, together with a data description file (*COV3ER_2016_dataset-description.xlsx*), and a script for reading and plotting the data (*COV3ER_2016_dataset_make_graphs.R*). The data and code to visualise are available here: <https://data.inrae.fr/dataset.xhtml?persistentId=doi:10.15454/IRZ9XX> .

Supplement link

825 Supplementary material includes a pdf document with supplementary figures and tables, and an Excel file containing the averaged fluxes, mixing ratios, LODf (**Table S3**). Also available are three CSV files containing correlation tables between VOCs (**Tables S4a, b, c**).

Authors contribution

Benjamin Loubet: Conceptualization, data curation, formal analysis, funding acquisition, Investigation, Methodology, project administration, software, supervision, validation, visualization, writing-original draft,
830 writing-review and editing. **Pauline Buysse**: Investigation, Data curation, Resources, writing - review & editing. **Lais Gonzaga-Gomez**: formal analysis, investigation, Software, writing - review & editing. **Florence Lafouge**: Investigation, Data curation, Resources, writing - review & editing. **Raluca Ciuraru**: Investigation, Resources, validation, writing - review & editing. **Céline Decuq**: Data Curation, Investigation, Resources, validation. **Julien Kammer**: Data Curation, Investigation, Resources, validation, writing - review & editing. **Sandy Bsaibes**: writing
835 - review & editing. **Christophe Boissard**: Resources. **Brigitte Durand**: Resources, investigation. **Jean-**

Christophe Gueudet: Resources. **Olivier Fanucci:** Resources. **Olivier Zurfluh:** Resources. **Letizia Abis:** formal analysis, investigation, software, writing - review & editing. **Nora Zannoni:** Investigation, writing - review & editing. **François Truong:** Resources, investigation. **Dominique Baisnée:** Resources, investigation. **Roland-Sarda Esteve:** Resources. **Michael Staudt:** writing - review & editing. **Valérie Gros:** Supervision, Resources, funding acquisition, investigation, methodology, writing - review & editing.

Competing interests

The authors declare that they have no conflict of interest.

Acknowledgements

We acknowledge funding by ADEME (COV3ER, n°1562C0032), ANAEE-FR services (ANR project n°11-INBS-0001). The data analysis was supported by the regional funding R2DS and the ADEME projects DICOV (grant n°1662c0020), AGRIMULTUPOL (grant number 1703C0012). Sandy Bsaibes acknowledges the European Union's Horizon 2020 research and innovation program under the Marie-Sklodowska-Curie grant agreement No 674911-IMPACT. The measurements were performed on the ICOS FR-GRI site. We acknowledge Dominique Tristan for letting access to the field.

References

- Abis, L. et al., 2018. Profiles of volatile organic compound emissions from soils amended with organic waste products. *Sci Total Environ*, 636: 1333-1343.
- Ammann, C., Brunner, A., Spirig, C. and Neftel, A., 2006. Technical note: Water vapour concentration and flux measurements with PTR-MS. *Atmospheric Chemistry and Physics*, 6: 4643-4651.
- Ashmore, M.R., 2005. Assessing the future global impacts of ozone on vegetation. *Plant Cell and Environment*, 28(8): 949-964.
- Aubinet, M. et al., 2000. Estimates of the annual net carbon and water exchange of forests: The EUROFLUX methodology. *Advances in Ecological Research*, Vol 30, 30: 113-175.
- Avnery, S., Mauzerall, D.L., Liu, J.F. and Horowitz, L.W., 2011. Global crop yield reductions due to surface ozone exposure: 1. Year 2000 crop production losses and economic damage. *Atmospheric Environment*, 45(13): 2284-2296.
- Baasandorj, M., Millet, D.B., Hu, L., Mitroo, D. and Williams, B.J., 2015. Measuring acetic and formic acid by proton-transfer-reaction mass spectrometry: sensitivity, humidity dependence, and quantifying interferences. *Atmospheric Measurement Techniques*, 8(3): 1303-1321.
- Bachy, A. et al., 2020. Dynamics and mechanisms of volatile organic compound exchanges in a winter wheat field. *Atmospheric Environment*, 221.
- Bachy, A. et al., 2018. Methanol exchange dynamics between a temperate cropland soil and the atmosphere. *Atmospheric Environment*, 176: 229-239.
- Bachy, A. et al., 2016. Are BVOC exchanges in agricultural ecosystems overestimated? Insights from fluxes measured in a maize field over a whole growing season. *Atmospheric Chemistry and Physics*, 16(8): 5343-5356.
- Bamberger, I. et al., 2010. BVOC fluxes above mountain grassland. *BIOGEOSCIENCES*, 7(5): 1413-1424.
- Bamberger, I. et al., 2011. Deposition fluxes of terpenes over grassland. *Journal of Geophysical Research*, 116(D14).
- Batten, J.H., Stutte, G.W. and Wheeler, R.M., 1995. Effect of crop development on biogenic emissions from plant populations grown in closed plant growth chambers. *Phytochemistry*, 39(6): 1351-7.
- Berhongaray, G., Verlinden, M.S., Broeckx, L.S., Janssens, I.A. and Ceulemans, R., 2017. Soil carbon and belowground carbon balance of a short-rotation coppice: assessments from three different approaches. *Global Change Biology Bioenergy*, 9(2): 299-313.

- 880 Brilli, F. et al., 2016. Rapid leaf development drives the seasonal pattern of volatile organic compound (VOC) fluxes in a 'coppiced' bioenergy poplar plantation. *Plant Cell and Environment*, 39(3): 539-555.
- Carozzi, M., Loubet, B., Acutis, M., Rana, G. and Ferrara, R.M., 2013. Inverse dispersion modelling highlights the efficiency of slurry injection to reduce ammonia losses by agriculture in the Po Valley (Italy). *Agricultural and Forest Meteorology*, 171: 306-318.
- 885 Carrión, O. et al., 2017. Methanethiol-dependent dimethylsulfide production in soil environments. *The ISME Journal*, 11(10): 2379-2390.
- Cojocariu, C. et al., 2005. The effect of ozone on the emission of carbonyls from leaves of adult *Fagus sylvatica*. *Plant Cell and Environment*, 28(5): 603-611.
- Copeland, N., Cape, J.N. and Heal, M.R., 2012. Volatile organic compound emissions from *Miscanthus* and short rotation coppice willow bioenergy crops. *Atmospheric Environment*, 60: 327-335.
- 890 Crespo, E. et al., 2013. Volatile organic compound emissions from elephant grass and bamboo cultivars used as potential bioethanol crop. *Atmospheric Environment*, 65: 61-68.
- Custer, T. and Schade, G., 2007. Methanol and acetaldehyde fluxes over ryegrass. *Tellus Series B-Chemical and Physical Meteorology*, 59(4): 673-684.
- 895 Das, M. et al., 2003. Measurements of hydrocarbon air-surface exchange rates over maize. *Atmospheric Environment*, 37(16): 2269-2277.
- Davison, B. et al., 2008. Cut-induced VOC emissions from agricultural grasslands. *Plant Biology*, 10(1): 76-85.
- De Gouw, J.A., Howard, C.J., Custer, T.G., Baker, B.M. and Fall, R., 2000. Proton-transfer chemical-ionization mass spectrometry allows real-time analysis of volatile organic compounds released from cutting and drying of crops. *Environmental Science & Technology*, 34(12): 2640-2648.
- 900 Effmert, U., Kalderas, J., Warnke, R. and Piechulla, B., 2012. Volatile Mediated Interactions Between Bacteria and Fungi in the Soil. *Journal of Chemical Ecology*, 38(6): 665-703.
- Eller, A.S.D. et al., 2011. Volatile organic compound emissions from switchgrass cultivars used as biofuel crops. *Atmospheric Environment*, 45(19): 3333-3337.
- 905 Fall, R., Albritton, D.L., Fehsenfeld, F.C., Kuster, W.C. and Goldan, P.D., 1988. Laboratory studies of some environmental variables controlling sulfur emissions from plants. *Journal of Atmospheric Chemistry*, 6(4): 341-362.
- Fares, S., Oksanen, E., Lannenpaa, M., Julkunen-Tiitto, R. and Loreto, F., 2010. Volatile emissions and phenolic compound concentrations along a vertical profile of *Populus nigra* leaves exposed to realistic ozone concentrations. *Photosynthesis Research*, 104(1): 61-74.
- 910 Fares, S. et al., 2012. Seasonal cycles of biogenic volatile organic compound fluxes and concentrations in a California citrus orchard. *Atmospheric Chemistry and Physics*, 12(20): 9865-9880.
- Feilberg, A., Bildsoe, P. and Nyord, T., 2015. Application of PTR-MS for Measuring Odorant Emissions from Soil Application of Manure Slurry. *Sensors*, 15(1): 1148-1167.
- 915 Filella, I., Wilkinson, M.J., Llusia, J., Hewitt, C.N. and Penuelas, J., 2007. Volatile organic compounds emissions in Norway spruce (*Picea abies*) in response to temperature changes. *Physiologia Plantarum*, 130(1): 58-66.
- Fruekilde, P., Hjorth, J., Jensen, N.R., Kotzias, D. and Larsen, B., 1998. Ozonolysis at vegetation surfaces: A source of acetone, 4-oxopentanal, 6-methyl-5-hepten-2-one, and geranyl acetone in the troposphere. *Atmospheric Environment*, 32(11): 1893-1902.
- 920 Gabriel, R., Schafer, L., Gerlach, C., Rausch, T. and Kesselmeier, J., 1999. Factors controlling the emissions of volatile organic acids from leaves of *Quercus ilex* L. (Holm oak). *Atmospheric Environment*, 33(9): 1347-1355.
- Gallagher, M.W. et al., 2000. Assessment of a relaxed eddy accumulation for measurements of fluxes of biogenic volatile organic compounds: study over arable crops and a mature beech forest. *Atmospheric Environment*, 34(18): 2887-2899.
- 925 Gitelson, II, Tikhomirov, A.A., Parshina, O.V., Ushakova, S.A. and Kalacheva, G.S., 2003. Volatile metabolites of higher plant crops as a photosynthesizing life support system component under temperature stress at different light intensities. In: M. Nelson, N.S. Pechurkin, W.F. Dempster, L.A. Somova and M.A. Shea (Editors), *Space Life Sciences: Closed Artificial Ecosystems and Life Support Systems*. *Advances in Space Research*, pp. 1781-1786.
- 930 Gomez, L.G. et al., 2021. Effect of senescence on biogenic volatile organic compound fluxes in wheat plants. *Atmospheric Environment*, 266: 118665.
- Gonzaga Gomez, L. et al., 2019. Comparative study of biogenic volatile organic compounds fluxes by wheat, maize and rapeseed with dynamic chambers over a short period in northern France. *Atmospheric Environment*, 214: 116855.
- 935 Graus, M. et al., 2011. Comparison of VOC emissions from conventional and alternative biofuel crops. *Abstracts of Papers of the American Chemical Society*, 242.

- 940 Graus, M. et al., 2013. Biosphere-atmosphere exchange of volatile organic compounds over C4 biofuel crops. *Atmospheric Environment*, 66: 161-168.
- Groene, T., 1995. Biogenic Production and Consumption of Dimethylsulfide (Dms) and Dimethylsulfoniopropionate (Dmsp) in the Marine Epipelagic Zone - a Review. *J Marine Syst*, 6(3): 191-209.
- 945 Guenther, A.B. et al., 2012. The Model of Emissions of Gases and Aerosols from Nature version 2.1 (MEGAN2.1): an extended and updated framework for modeling biogenic emissions. *Geoscientific Model Development*, 5(6): 1471-1492.
- Hafner, S.D., Montes, F., Rotz, C.A. and Mitloehner, F., 2010. Ethanol emission from loose corn silage and exposed silage particles. *Atmospheric Environment*, 44(34): 4172-4180.
- 950 Hatch, L.E. et al., 2017. Multi-instrument comparison and compilation of non-methane organic gas emissions from biomass burning and implications for smoke-derived secondary organic aerosol precursors. *Atmospheric Chemistry and Physics*, 17(2): 1471-1489.
- Haworth, M. et al., 2017. Moderate Drought Stress Induces Increased Foliar Dimethylsulphoniopropionate (DMSP) Concentration and Isoprene Emission in Two Contrasting Ecotypes of *Arundo donax*. *FRONTIERS IN PLANT SCIENCE*, 8.
- 955 Helmig, D. et al., 1998. Vertical profiling and determination of landscape fluxes of biogenic nonmethane hydrocarbons within the planetary boundary layer in the Peruvian Amazon. *Journal of Geophysical Research-Atmospheres*, 103(D19): 25519-25532.
- Hobbs, P.J., Webb, J., Mottram, T.T., Grant, B. and Misselbrook, T.M., 2004. Emissions of volatile organic compounds originating from UK livestock agriculture. *Journal of the Science of Food and Agriculture*, 84(11): 1414-1420.
- 960 Holopainen, J.K., Kivimaenpaa, M. and Nizkorodov, S.A., 2017. Plant-derived Secondary Organic Material in the Air and Ecosystems. *Trends in Plant Science*, 22(9): 744-753.
- IPCC, 2018. IPCC, 2018: Global Warming of 1.5°C. An IPCC Special Report on the impacts of global warming of 1.5°C above pre-industrial levels and
- 965 related global greenhouse gas emission pathways, in the context of strengthening the global response to the threat of climate change,
- sustainable development, and efforts to eradicate poverty [Masson-Delmotte, V., P. Zhai, H.-O. Pörtner, D. Roberts, J. Skea, P.R. Shukla,
- 970 A. Pirani, W. Moufouma-Okia, C. Péan, R. Pidcock, S. Connors, J.B.R. Matthews, Y. Chen, X. Zhou, M.I. Gomis, E. Lonnoy, T. Maycock,
- M. Tignor, and T. Waterfield (eds.)]. Intergovernmental Panel on Climate Change.
- Jacob, D.J. et al., 2005. Global budget of methanol: Constraints from atmospheric observations. *Journal of Geophysical Research-Atmospheres*, 110(D8).
- Jardine, K. et al., 2011. Ecosystem-scale compensation points of formic and acetic acid in the central Amazon. *Biogeosciences*, 8(12): 3709-3720.
- 975 Jardine, K. et al., 2015. Dimethyl sulfide in the Amazon rain forest. *Global Biogeochemical Cycles*, 29(1): 19-32.
- Jud, W. et al., 2016. Plant surface reactions: an opportunistic ozone defence mechanism impacting atmospheric chemistry. *Atmospheric Chemistry and Physics*, 16(1): 277-292.
- Kammer, J. et al., 2020. Characterization of particulate and gaseous pollutants from a French dairy and sheep farm. *Science of the Total Environment*, 712.
- 980 Kanda, K.-i., Tsuruta, H. and Minami, K., 1995. Emissions of biogenic sulfur gases from maize and wheat fields. *Soil Science and Plant Nutrition*, 41(1): 1-8.
- Karl, M., Guenther, A., Koble, R., Leip, A. and Seufert, G., 2009a. A new European plant-specific emission inventory of biogenic volatile organic compounds for use in atmospheric transport models. *Biogeosciences*, 6(6): 1059-1087.
- 985 Karl, T., Curtis, A.J., Rosenstiel, T.N., Monson, R.K. and Fall, R., 2002. Transient releases of acetaldehyde from tree leaves - products of a pyruvate overflow mechanism? *Plant Cell and Environment*, 25(9): 1121-1131.
- Karl, T. et al., 2001. Eddy covariance measurements of oxygenated volatile organic compound fluxes from crop harvesting using a redesigned proton-transfer-reaction mass spectrometer. *Journal of Geophysical Research-Atmospheres*, 106(D20): 24157-24167.
- 990 Karl, T. et al., 2009b. Rapid formation of isoprene photo-oxidation products observed in Amazonia. *Atmospheric Chemistry and Physics*, 9(20): 7753-7767.
- Karl, T. et al., 2012. Selective measurements of isoprene and 2-methyl-3-buten-2-ol based on NO⁺ ionization mass spectrometry. *Atmospheric Chemistry and Physics*, 12(24): 11877-11884.
- 995 Karl, T. et al., 2010. Efficient Atmospheric Cleansing of Oxidized Organic Trace Gases by Vegetation. *Science*, 330(6005): 816-819.
- Karl, T. et al., 2005. Senescing grass crops as regional sources of reactive volatile organic compounds. *Journal of Geophysical Research-Atmospheres*, 110(D15).

- Keenan, T., Niinemets, U., Sabate, S., Gracia, C. and Penuelas, J., 2009. Process based inventory of isoprenoid emissions from European forests: model comparisons, current knowledge and uncertainties. *Atmospheric Chemistry and Physics*, 9(12): 4053-4076.
- Keskitalo, J., Bergquist, G., Gardestrom, P. and Jansson, S., 2005. A cellular timetable of autumn senescence. *Plant Physiology*, 139(4): 1635-1648.
- Kesselmeier, J., Bode, K., Gerlach, C. and Jork, E.M., 1998. Exchange of atmospheric formic and acetic acids with trees and crop plants under controlled chamber and purified air conditions. *Atmospheric Environment*, 32(10): 1765-1775.
- Kiraly, Z., 1962. Phenol Content in Rust Infected and Nitrogen Fertilized Wheat Leaves. *Phytopathology*, 52(8): 738-&.
- Konig, G. et al., 1995. Relative Contribution of Oxygenated Hydrocarbons to the Total Biogenic Voc Emissions of Selected Mid-European Agricultural and Natural Plant-Species. *Atmospheric Environment*, 29(8): 861-874.
- Kormann, R. and Meixner, F.X., 2001. An analytical footprint model for non-neutral stratification. *Boundary-Layer Meteorology*, 99(2): 207-224.
- Koss, A.R. et al., 2018. Non-methane organic gas emissions from biomass burning: identification, quantification, and emission factors from PTR-ToF during the FIREX 2016 laboratory experiment. *Atmospheric Chemistry and Physics*, 18(5): 3299-3319.
- Kreuzwieser, J. et al., 2001. Acetaldehyde emission by the leaves of trees – correlation with physiological and environmental parameters. *Physiologia Plantarum*, 113(1): 41-49.
- Laffineur, Q. et al., 2012. Abiotic and biotic control of methanol exchanges in a temperate mixed forest. *Atmospheric Chemistry and Physics*, 12(1): 577-590.
- Lang-Yona, N. et al., 2010. The chemical and microphysical properties of secondary organic aerosols from Holm Oak emissions. *Atmospheric Chemistry and Physics*, 10(15): 7253-7265.
- Langford, B., Acton, W., Ammann, C., Valach, A. and Nemitz, E., 2015. Eddy-covariance data with low signal-to-noise ratio: time-lag determination, uncertainties and limit of detection. *Atmos. Meas. Tech.*, 8(10): 4197-4213.
- Lathièrè, J., Hewitt, C.N. and Beerling, D.J., 2010. Sensitivity of isoprene emissions from the terrestrial biosphere to 20th century changes in atmospheric CO₂ concentration, climate, and land use. *Global Biogeochemical Cycles*, 24(1).
- Laufs, S. et al., 2016. Diurnal fluxes of HONO above a crop rotation. *Atmos. Chem. Phys. Discuss.*, 2016: 1-28.
- Leuning, R., 2007. The correct form of the Webb, Pearman and Leuning equation for eddy fluxes of trace gases in steady and non-steady state, horizontally homogeneous flows. *Boundary-Layer Meteorology*, 123(2): 263-267.
- Link, M.F., Nguyen, T.B., Bates, K., Müller, J.-F. and Farmer, D.K., 2020. Can Isoprene Oxidation Explain High Concentrations of Atmospheric Formic and Acetic Acid over Forests? *ACS Earth and Space Chemistry*, 4(5): 730-740.
- Loubet, B. et al., 2018. Evaluation of a new inference method for estimating ammonia volatilisation from multiple agronomic plots. *Biogeosciences*, 15(11): 3439-3460.
- Loubet, B. et al., 2012. Investigating the stomatal, cuticular and soil ammonia fluxes over a growing tritical crop under high acidic loads. *Biogeosciences*, 9(4): 1537-1552.
- Loubet, B. et al., 2010. An inverse model to estimate ammonia emissions from fields. *European Journal of Soil Science*, 61(5): 793-805.
- Loubet, B. et al., 2011. Carbon, nitrogen and Greenhouse gases budgets over a four years crop rotation in northern France. *Plant and Soil*, 343(1-2): 109-137.
- Makkonen, R. et al., 2012. Air pollution control and decreasing new particle formation lead to strong climate warming. *Atmospheric Chemistry and Physics*, 12(3): 1515-1524.
- Messina, P. et al., 2016. Global biogenic volatile organic compound emissions in the ORCHIDEE and MEGAN models and sensitivity to key parameters. *Atmospheric Chemistry and Physics*, 16(22): 14169-14202.
- Mielnik, A., Link, M., Mattila, J., Fulgham, S.R. and Farmer, D.K., 2018. Emission of formic and acetic acids from two Colorado soils. *Environmental Science-Processes & Impacts*, 20(11): 1537-1545.
- Miresmaili, S. et al., 2013. Impacts of herbaceous bioenergy crops on atmospheric volatile organic composition and potential consequences for global climate change. *Global Change Biology Bioenergy*, 5(4): 375-383.
- Misztal, P.K., Heal, M.R., Nemitz, E. and Cape, J.N., 2012. Development of PTR-MS selectivity for structural isomers: Monoterpenes as a case study. *International Journal of Mass Spectrometry*, 310: 10-19.
- Misztal, P.K. et al., 2014. Airborne flux measurements of biogenic isoprene over California. *Atmospheric Chemistry and Physics*, 14(19): 10631-10647.
- Monks, P.S. et al., 2015. Tropospheric ozone and its precursors from the urban to the global scale from air quality to short-lived climate forcer. *Atmos. Chem. Phys.*, 15(15): 8889-8973.

- Montes, F., Hafner, S.D., Rotz, C.A. and Mitloehner, F.M., 2010. Temperature and air velocity effects on ethanol emission from corn silage with the characteristics of an exposed silo face. *Atmospheric Environment*, 44(16): 1987-1995.
- 1060 Morrison, E.C., Drewer, J. and Heal, M.R., 2016. A comparison of isoprene and monoterpene emission rates from the perennial bioenergy crops short-rotation coppice willow and *Miscanthus* and the annual arable crops wheat and oilseed rape. *Global Change Biology Bioenergy*, 8(1): 211-225.
- Mozaffar, A. et al., 2018. Biogenic volatile organic compound emissions from senescent maize leaves and a comparison with other leaf developmental stages. *Atmospheric Environment*, 176: 71-81.
- 1065 Muller, M. et al., 2010. First eddy covariance flux measurements by PTR-TOF. *Atmospheric Measurement Techniques*, 3(2): 387-395.
- Nguyen, T.B. et al., 2015. Rapid deposition of oxidized biogenic compounds to a temperate forest. *Proc Natl Acad Sci U S A*, 112(5): E392-401.
- 1070 Ni, J.-Q., Robarge, W.P., Xiao, C. and Heber, A.J., 2012. Volatile organic compounds at swine facilities: A critical review. *Chemosphere*, 89(7): 769-788.
- Niinemets, U., Fares, S., Harley, P. and Jardine, K.J., 2014. Bidirectional exchange of biogenic volatiles with vegetation: emission sources, reactions, breakdown and deposition. *Plant Cell and Environment*, 37(8): 1790-1809.
- 1075 Niinemets, U. et al., 2011. Estimations of isoprenoid emission capacity from enclosure studies: measurements, data processing, quality and standardized measurement protocols. *Biogeosciences*, 8(8): 2209-2246.
- Pang, X., 2015. Biogenic volatile organic compound analyses by PTR-TOF-MS: Calibration, humidity effect and reduced electric field dependency. *Journal of Environmental Sciences*, 32: 196-206.
- Papageorgiou, A., Voutsas, D. and Papadakis, N., 2014. Occurrence and fate of ozonation by-products at a full-scale drinking water treatment plant. *SCIENCE OF THE TOTAL ENVIRONMENT*, 481: 392-400.
- 1080 Park, J.-H. et al., 2013a. Active Atmosphere-Ecosystem Exchange of the Vast Majority of Detected Volatile Organic Compounds. *Science*, 341(6146): 643-647.
- Park, J.H. et al., 2013b. Eddy covariance emission and deposition flux measurements using proton transfer reaction - time of flight - mass spectrometry (PTR-TOF-MS): comparison with PTR-MS measured vertical gradients and fluxes. *Atmospheric Chemistry and Physics*, 13(3): 1439-1456.
- 1085 Personne, E. et al., 2015. Investigating sources and sinks for ammonia exchanges between the atmosphere and a wheat canopy following slurry application with trailing hose. *Agricultural and Forest Meteorology*, 207: 11-23.
- Portillo-Estrada, M., Ariza-Carricondo, C. and Ceulemans, R., 2020. Outburst of senescence-related VOC emissions from a bioenergy poplar plantation. *Plant Physiology and Biochemistry*, 148: 324-332.
- 1090 Portillo-Estrada, M., Zenone, T., Arriga, N. and Ceulemans, R., 2018. Contribution of volatile organic compound fluxes to the ecosystem carbon budget of a poplar short-rotation plantation. *Global Change Biology Bioenergy*, 10(6): 405-414.
- Potier, E. et al., 2017. Chemical reaction rates of ozone in water infusions of wheat, beech, oak and pine leaves of different ages. *ATMOSPHERIC ENVIRONMENT*, 151: 176-187.
- 1095 Potier, E. et al., 2015. Multi layer modelling of ozone fluxes on winter wheat reveals large deposition on wet senescing leaves. *Agricultural and Forest Meteorology*, 211: 58-71.
- Rantala, P., Aalto, J., Taipale, R., Ruuskanen, T.M. and Rinne, J., 2015. Annual cycle of volatile organic compound exchange between a boreal pine forest and the atmosphere. *Biogeosciences*, 12(19): 5753-5770.
- 1100 Ruuskanen, T.M. et al., 2011. Eddy covariance VOC emission and deposition fluxes above grassland using PTR-TOF. *Atmospheric Chemistry and Physics*, 11(2): 611-625.
- Schade, G.W. and Goldstein, A.H., 2001. Fluxes of oxygenated volatile organic compounds from a ponderosa pine plantation. *Journal of Geophysical Research-Atmospheres*, 106(D3): 3111-3123.
- Scholler, C.E.G., Gurtler, H., Pedersen, R., Molin, S. and Wilkins, K., 2002. Volatile metabolites from actinomycetes. *Journal of Agricultural and Food Chemistry*, 50(9): 2615-2621.
- 1105 Seco, R., Penuelas, J. and Filella, I., 2007. Short-chain oxygenated VOCs: Emission and uptake by plants and atmospheric sources, sinks, and concentrations. *Atmospheric Environment*, 41(12): 2477-2499.
- Seinfeld, J.H. and Pandis, S.N., 1998. *Atmospheric chemistry and physics. From air pollution to climate change.* Wiley-Interscience, 1326 pp.
- 1110 Sindelarova, K. et al., 2014. Global data set of biogenic VOC emissions calculated by the MEGAN model over the last 30 years. *Atmospheric Chemistry and Physics*, 14(17): 9317-9341.
- Spirig, C. et al., 2005. Eddy covariance flux measurements of biogenic VOCs during ECHO 2003 using proton transfer reaction mass spectrometry. *Atmospheric Chemistry and Physics*, 5: 465-481.
- 1115 Staudt, M., Wolf, A. and Kesselmeier, J., 2000. Influence of environmental factors on the emissions of gaseous formic and acetic acids from orange (*Citrus sinensis* L.) foliage. *Biogeochemistry*, 48(2): 199-216.

- Steeghs, M.M.L., Crespo, E. and Harren, F.J.M., 2007. Collision induced dissociation study of 10 monoterpenes for identification in trace gas measurements using the newly developed proton-transfer reaction ion trap mass spectrometer. *International Journal of Mass Spectrometry*, 263(2-3): 204-212.
- 1120 Stella, P. et al., 2013. Assessment of the total, stomatal, cuticular, and soil 2 year ozone budgets of an agricultural field with winter wheat and maize crops. *Journal of Geophysical Research-Biogeosciences*, 118(3): 1120-1132.
- Stockwell, C.E., 2016. Advanced measurements of undersampled globally significant biomass burning sources, University of Montana, Montana, USA.
- 1125 Sulzer, P. et al., 2014. A Proton Transfer Reaction-Quadrupole interface Time-Of-Flight Mass Spectrometer (PTR-QiTOF): High speed due to extreme sensitivity. *International Journal of Mass Spectrometry*, 368: 1-5.
- Tani, A., Hayward, S., Hansel, A. and Hewitt, C.N., 2004. Effect of water vapour pressure on monoterpene measurements using proton transfer reaction-mass spectrometry (PTR-MS). *International Journal of Mass Spectrometry*, 239(2-3): 161-169.
- 1130 Tani, A., Hayward, S. and Hewitt, C.N., 2003. Measurement of monoterpenes and related compounds by proton transfer reaction-mass spectrometry (PTR-MS). *International Journal of Mass Spectrometry*, 223(1-3): 561-578.
- Tuzet, A., Perrier, A., Loubet, B. and Cellier, P., 2011. Modelling ozone deposition fluxes: The relative roles of deposition and detoxification processes. *Agricultural and Forest Meteorology*, 151(4): 480-492.
- 1135 Venneman, J. et al., 2020. Respiratory CO₂ Combined With a Blend of Volatiles Emitted by Endophytic *Serendipita* Strains Strongly Stimulate Growth of *Arabidopsis* Implicating Auxin and Cytokinin Signaling. *Frontiers in Plant Science*, 11(1343).
- Vettikatt, L. et al., 2020. Significant emissions of dimethyl sulfide and monoterpenes by big-leaf mahogany trees: discovery of a missing dimethyl sulfide source to the atmospheric environment. *Atmospheric Chemistry and Physics*, 20(1): 375-389.
- 1140 Vlasenko, A., Macdonald, A.M., Sjostedt, S.J. and Abbatt, J.P.D., 2010. Formaldehyde measurements by Proton transfer reaction - Mass Spectrometry (PTR-MS): correction for humidity effects. *Atmospheric Measurement Techniques*, 3(4): 1055-1062.
- Vuolo, R.M. et al., 2017. Nitrogen oxides and ozone fluxes from an oilseed-rape management cycle: the influence of cattle slurry application. *BIOGEOSCIENCES*, 14(8): 2225-2244.
- 1145 Warneke, C. et al., 1999. Acetone, methanol, and other partially oxidized volatile organic emissions from dead plant matter by abiological processes: Significance for atmospheric HO_x chemistry. *GLOBAL BIOGEOCHEMICAL CYCLES*, 13(1): 9-17.
- Webb, E.K., Pearman, G.I. and Leuning, R., 1980. Correction of flux measurements for density effects due to heat and water vapour transfer. *Quarterly Journal of the Royal Meteorological Society*, 106(447): 85-100.
- 1150 Wiss, F. et al., 2017. Net ecosystem fluxes and composition of biogenic volatile organic compounds over a maize field-interaction of meteorology and phenological stages. *Global Change Biology Bioenergy*, 9(11): 1627-1643.
- Woo, H.R., Kim, H.J., Lim, P.O. and Nam, H.G., 2019. Leaf Senescence: Systems and Dynamics Aspects. In: S.S. Merchant (Editor), *Annual Review of Plant Biology*, Vol 70. *Annual Review of Plant Biology*, pp. 347-376.
- 1155 Xiong, J., He, Z., Tang, X., Misztal, P.K. and Goldstein, A.H., 2019. Modeling the Time-Dependent Concentrations of Primary and Secondary Reaction Products of Ozone with Squalene in a University Classroom. *Environ Sci Technol*, 53(14): 8262-8270.
- Yáñez-Serrano, A.M. et al., 2021. GLOVOCS - Master compound assignment guide for proton transfer reaction mass spectrometry users. *Atmospheric Environment*, 244: 117929.
- 1160 Yonemura, S. et al., 2005. Uptake of carbonyl sulfide (COS) and emission of dimethyl sulfide (DMS) by plants. *PHYTON-ANNALES REI BOTANICAE*, 45(4, SI): 17-24.
- Zenone, T. et al., 2016. Interaction between isoprene and ozone fluxes in a poplar plantation and its impact on air quality at the European level. *Scientific Reports*, 6.
- 1165 Zhao, J. et al., 2016. Volatile organic compound emissions from straw-amended agricultural soils and their relations to bacterial communities: A laboratory study. *Journal of Environmental Sciences*, 45: 257-269.
- Zhou, P.T. et al., 2017. Boreal forest BVOC exchange: emissions versus in-canopy sinks. *Atmospheric Chemistry and Physics*, 17(23): 14309-14332.